Response to Anonymous Referee #1

We thank the reviewer for his/her constructive comments and suggestions on this manuscript, which are very helpful for us to improve our paper. Our responses to these comments are given below.

- *The authors outline a radar cloud detection algorithm, apply it to simulated data, process 2 months of real data and show comparisons to ARM's operational cloud radar detection. The authors conclude that their algorithm is an improvement since it detects more clouds. Overall, there needs to be more done to show that the algorithm in indeed "new and improved" as they state repeatedly throughout the manuscript. As is, the study presents a slightly-modified detection algorithm, applies it to a small amount of real data without concretely showing if the increased detection represents a true improvement.*

Response: Our hydrometeor detection method first involves convolving the SNR image with a 2-D Gaussian filter to suppress the noise and selecting a proper SNR threshold to separate noise from signal. Since this method does not apply a spatial filter at the initial stage as in previous studies, it can reduce the tendency of removing cloud corners. Figure 1 shows that a threshold of 2.8 can keep a low false positive of 0.12% and a false negative of 2.52%. By aiming to recognize more hydrometeors (e.g. clouds with weak SNR) and maintain sharp cloud edges, the Gaussian filter with the bilateral filter enhances the contrast between weak signal and noise and preserve sharp cloud edges. In our method, the Gaussian filter with the bilateral filter, which has not been applied before, is followed by a spatial filter with a central weighting to further reduce both false positive and false negative. Following the reviewer's suggestion, we apply our radar cloud detection algorithm to longer periods of real data and compare with more MPL observations. We show that our method indeed improves cloud detection.

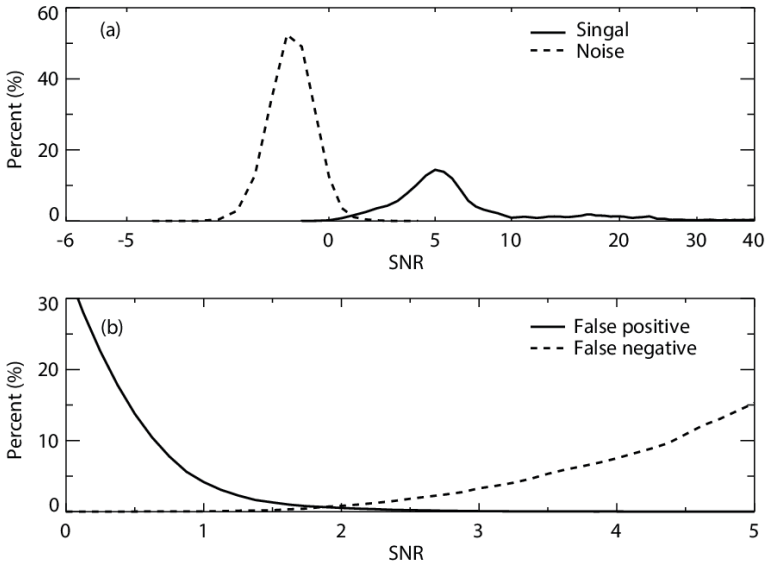

Figure 1. (a) SNR distribution of the noise and signal after convolving with a 3×3

Gaussian kernel, averaged from three simulated "square clouds" that have strong, medium and weak SNR values and random Gaussian noise. Both the noise and cloud signals are sampled from KAZR observation at the SACOL with SNR value from weak to strong; (b) false positive and false negative as a function of SNR threshold.

- The manuscript seems to claim that using the SNR for detection is better than previous work since SNR is Gaussian-distributed. First, the authors show the skewness of the noise distribution to be near-zero and conclude that the distribution is Gaussian. A skewness of zero is a necessary but not sufficient condition for a Gaussian distribution: this only implies the distribution is symmetric. Instead one should show that the noise PDF is best-fit by a Gaussian PDF. Regardless of the actual distribution of the SNR, the transformation from power-space to SNR-space (i.e. Eq. (1)) before applying averaging and a thresholding mask is pointless. As long as the noise is randomly distributed, averaging like the authors do will still reduce the noise and a threshold can still be applied. A Gaussian-distributed weighted average (i.e. Eq. 2) can still be used on non Gaussian noise. The only new part of the algorithm is to applying an existing bilateral filter to avoid smearing edges of cloud boundaries.

Response: We did examine whether the SNR of noise satisfies a Gaussian distribution. Thank the reviewer for pointing this out. We have corrected the improper statement in the revised manuscript. We agree with the reviewer that a Gaussian-distribution weighted average can be used on non-Gaussian noise and can narrow the noise distribution as long as the noise is randomly distributed. However, it is necessary for our method to use a Gaussian-like distribution. We did not mean that the use of the SNR is better than previous work, but just pointed out that SNR is close to a Gaussian Distribution. The application of the bilateral filter function is based on calculating the probability for a given range of SNR values, which relies on the Gaussian distribution. We have modified this part in the revised manuscript to clarify these issues.

- The authors also assume that a higher rate of detection by their algorithm is an improvement over the ARM method. However, they do not demonstrate whether or not this increase is caused by an increase rate of false detections. I suggest that the authors use the MPL as a truth for cloud detection and compare both their algorithm and ARM's to that. Otherwise, there is no way of knowing if the cloud mask is truly improved.

Response: Thanks for this suggestion. We compare the radar cloud mask results derived from our method and ARM algorithm with the MPL detected features in January and July, 2014 when both radar and lidar observations are available. It is found that the increased detections by our method as compared with the ARM algorithm are mostly those also identified as features by MPL. Figure 2 shows an example in January 9, 2014. The green color represents the increased detections that are also identified as features by MPL while the red represents the increased detection that are not detected by MPL. The features that are not observed by MPL are mainly related to a total attenuation of lidar signals by optically thick clouds below or appear below the cloud

base from which large precipitating hydrometeors may fall out that can not be observed by MPL.

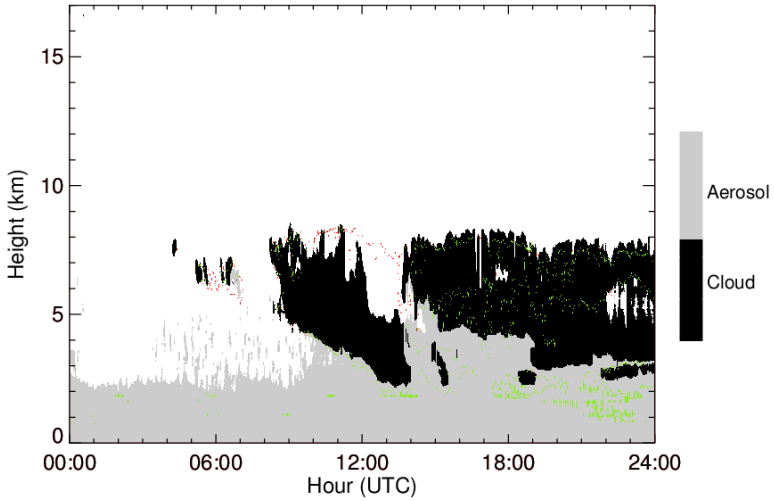

Figure 2. Increased hydrometeor detections by our algorithm versus ARM algorithm in comparison with the MPL feature mask in January 9, 2014. The black and gray regions represent the cloud and aerosol detected by MPL. The green part represents the increased detections that are also identified as features by MPL detection. The red part represents the increased detection that are not detected by MPL.

We analyzed data in January and July, 2014 when both KAZR and MPL observations are available, and showed the percentage of the increased detections identified by both KAZR with our method and MPL observations as compared to the total increased detections in Figure 3. We see that most of the increased detections are also detected as features by MPL. The percentage drops to a minimum of 70% at about 9 km, where the total increased cloud range bins are only about 110 and there are 35 range bins that are identified by our method are not observed by MPL. Considering all the increased detections by our method, 98.6% of them are confirmed by MPL as features.

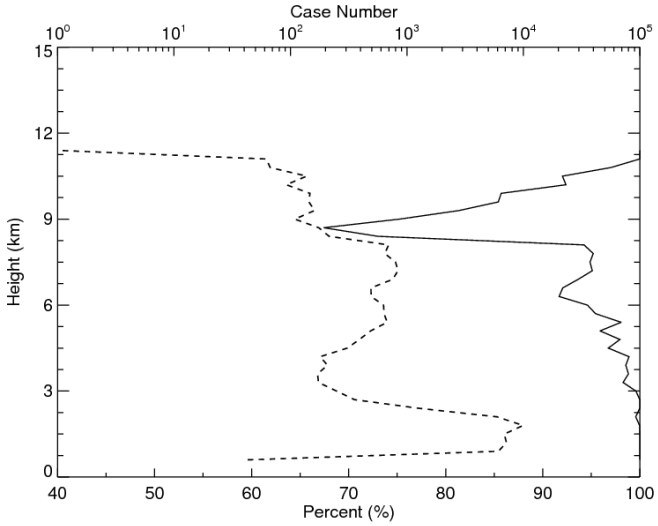

Figure 3. The solid line is the percentage of increased detections seen by both KAZR with our method and MPL as compared with the total increased detections. The dot line is the number of increased detections.

- I am particular considered about their increased detection around 2km since in their example (Fig. 6) many false positives exist at that height. The authors claim that this is dust since the MPL backscatter is larger, but the larger backscatter only exists near the surface. Most of the radar detections around 2km have lower backscatter and appear to be false positives. Even if they are dust, isn't it undesirable to have them in your cloud mask?

Response: Following the reviewer's suggestion, we examine the MPL depolarization ratio for the same case shown in the original Fig.6 in the manuscript. We found that the depolarization ratios of increased detections by our method are larger than those at surroundings, indicating the particles are very likely large dust particles. Figure 4 shows the depolarization ratio of MPL for January 8, 2014.

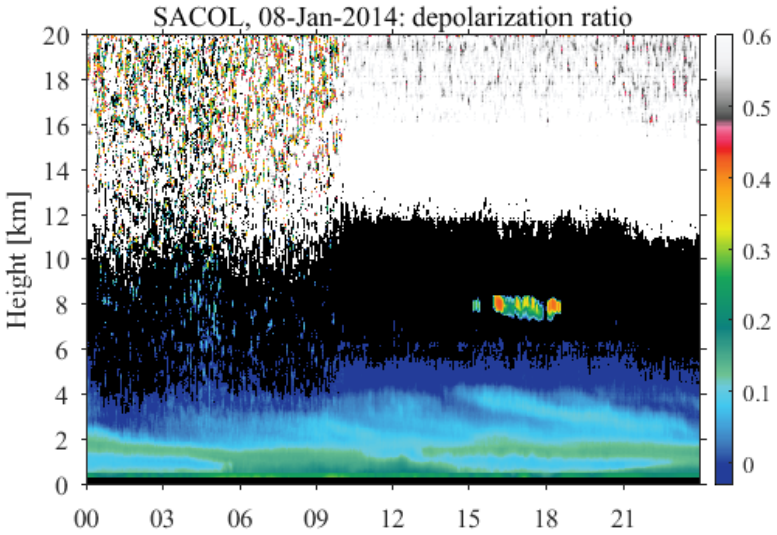

Figure 4. Depolarization ratio of MPL for January 8, 2014.

Although the dust is not desired for cloud mask, the appearance of those particles does prove the ability of our method on recognizing weak signals.

- I would also suggest that the author assess improvement using more than 2 months of data. Part of the strength of both the CloudSat and MMCR algorithms which the authors refer to is that they have process a lot of data between them.

Response: We applied our algorithm to six months of data including 3 months for summer and 3 months for winter, and our method is robust. See more in the following replies and related revisions of the manuscript.

- Some effort should also be made to compare to the newer ARM KAZR and ARM scanning radar cloud mask. The ARM MMCR are now longer used at any of the ARM sites.

Response: This is a good suggestion for our future work.

- A few other thoughts that would improve the manuscript. It would be instructive to see the steps of the detection method (i.e. Fig. 3) illustrated using an image of real data. Also, to aid in determining if you are detecting dust in the radar cloud mask, using the MPL depolarization instead of backscatter would identify dust more clearly. Finally I would suggest adding a confusion matrix as a complement to Fig. 7 would which show that any agreement there isn't due to some cancellation of errors

Response: Thanks for the suggestions. The observation of January 8th, 2014 is used to illustrate the steps of our detection method as shown in Figure 5. Figure 5a is the original SNR input. Figure 5b shows the SNR distribution after noise reduction process. We can see that the SNR distribution becomes much smoother than Fig. 5a. This step is crucial for the enhancement of the contrast between signal and noise. Figures 5c and 5d are results by applying the binary mask and using a spatial filter, respectively. We have added the MPL depolarization shown in Figure 4 to the Figure 6 in the manuscript. We have counted the number of range gates that are detected as noise by our method but signal by ARM algorithm, that are detected as signals by our method but noise by ARM, and that are detected by both for the expanded six months. The results are shown in the Figure 6. It is clear that the cancellation of errors can be negligible.

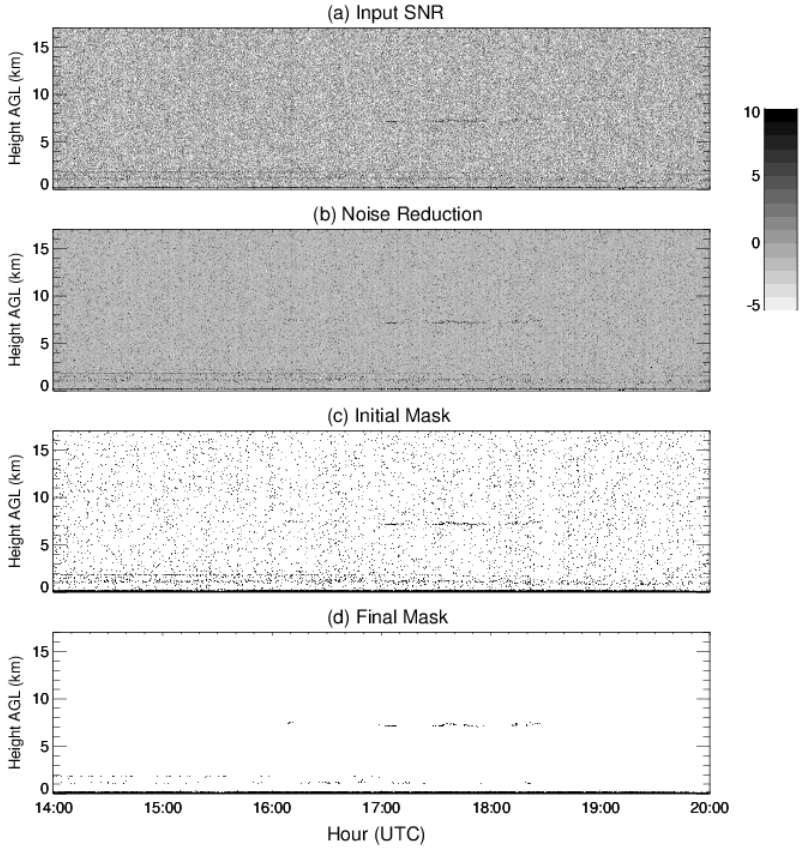

Figure 5. The illustration of the steps of our method for the case of January 8th, 2014.

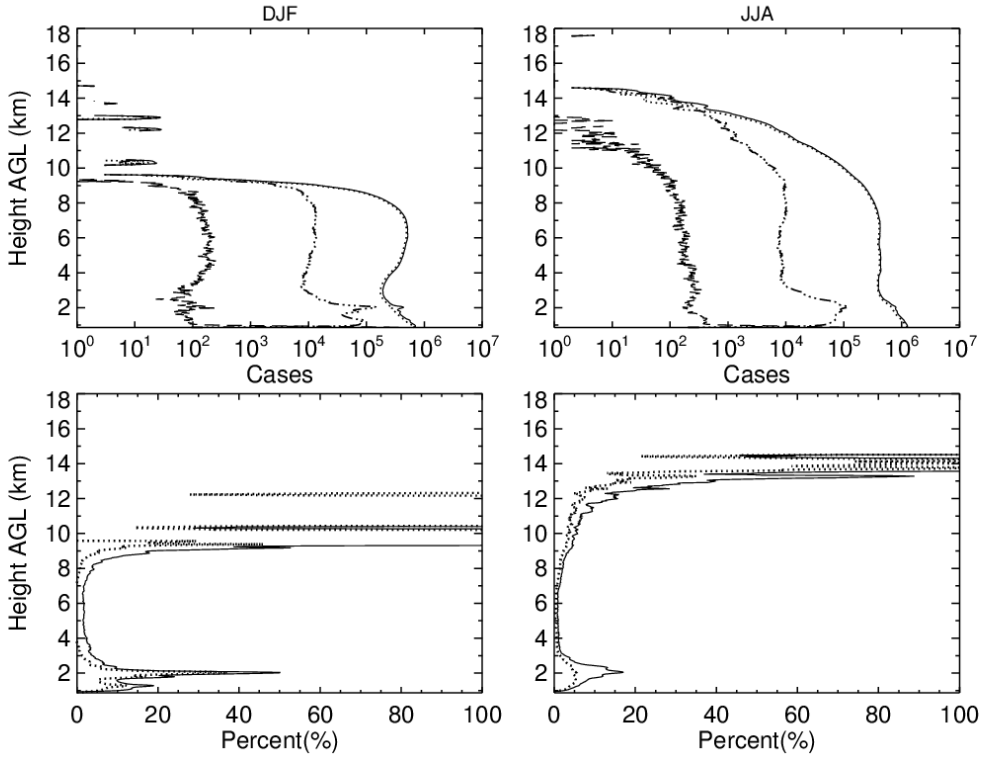

Figure 6. Same as the Figure 7 in the manuscript, but for six months. The dash lines in the upper two panels represent the number of range gates detected as noise by our method but signal by ARM. The dot-dash line is the increased number of range gates that are detected as signal by our method. The dot line, which is close to the solid line, represent the range gate number that are detected as signals by both methods. The solid line is the total number of bins that are identified by our method as signals.

MINOR COMMENTS
line 25: the authors does examine returns at various significance levels

Response: Sorry for the incorrect statement. We have modified this sentence as **"**A noise reduction scheme that can reduce noise distribution to a narrow range is proposed in order to detect cloud pixels with more weak signals. A spatial filter with central weighting, which is widely used in current cloud radar hydrometeor detection algorithms, is also employed in our method to examine radar return for significant levels of signals.**"**

line 27: change "reducing noise" to "reducing the noise"

Response: "the" is added.

line 29: remove comma

Response: comma is removed.

line 33: change "hydrometeor identifications" to "hydrometeor identifications in simulated clouds"

Response: We have made this change.

line 35-36: "move around our planet" is awkward wording

Response: "move around our planet" is deleted.

line 41: replace "stage of" with "component of"

Response: Replaced.

line 43: change "cannot be accurately represented" to "are difficult to represent"

Response: Changed.

line 50: change "models" to "models,"

Response: A comma is added.

line 60: remove "are powerful instruments"

Response: Removed.

line 63: change "and they have excellent sensitivity" to "making them sensitive"

Response: Changed.

line 68: change "in" to "at"

Response: Changed.
lines 71-76: Here you should also mention that the MMCR are no longer used by the ARM program and have been replaced with KAZR.

Response: We have mentioned that MMCRs have been replaced with KAZR at ARM sites.

line 86: remove successfully modified and

Response: Removed.

lines 88-95: all of this can be removed, none of this discussion is necessary

Response: We keep this part because the bilateral filter idea is applied to the cloud feature detection for the first time.

lines 95-96: don't understand the sentence here
Response: Here we mean that the cloud mask is similar to the image process. (i.e. effectively separate noise from target while keep its feature intact).

line 141: what are "internal and external sources"
Response: We refer the noise generated within the circuit that may be caused by changes of current or temperature as internal sources, and noise induced from the antenna as external sources.

Fig. 1a: why does the power "cutoff" at the high-end of the distribution
Response: It is because the noise power at the high-end of the distribution is larger than the maximum of the upper x axis. This issue is solved by expending the maximum to $8*10^{-13}$ as shown in the following figure.

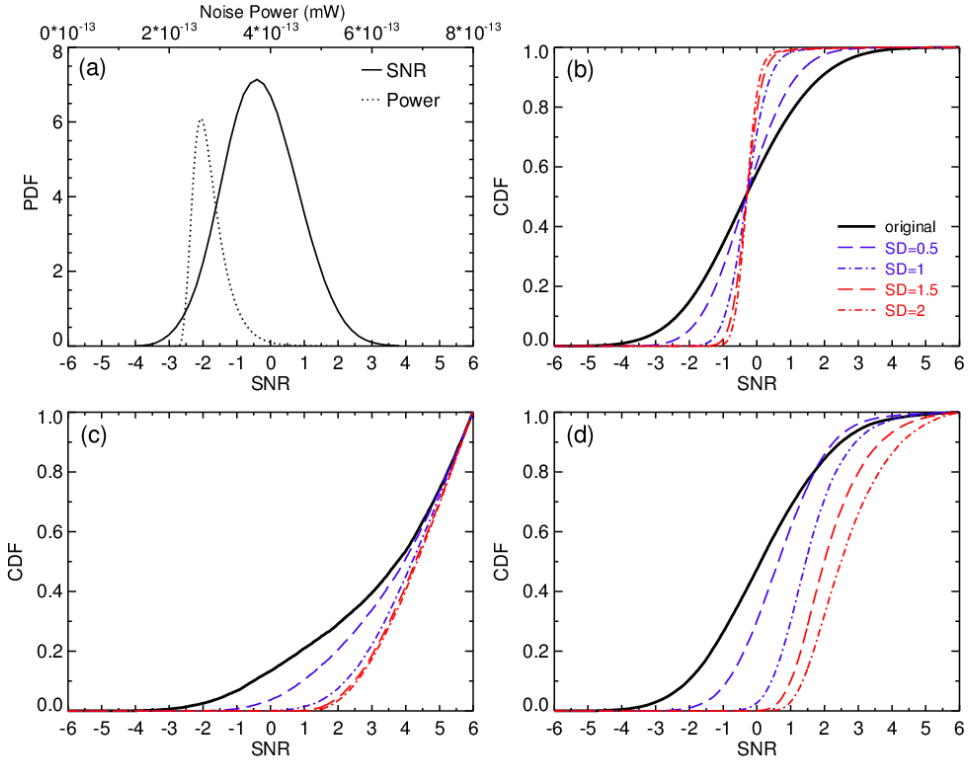

line 152-154: is there a reason to expect noise to be range dependent?

Response: Here we want to check the reason for the negative mean value of SNR.

line 157-158: change "randomly Gaussian distributed" to "random"

Response: Changed

line 187: "about three standard deviations" or "at three standard deviations"?

Response: not exactly at three standard deviations.

lines 188-203: most of this discussion is unnecessary: it is generally understood that average will reduce noise.

Response: Here would like to show large filter will also blur the boundary of cloud.

lines 207-208: clarify "cloudy or clear side"

Response: cloudy side means the central pixel is cloud signal, clear side means the central pixel belongs to noise.

line 213: replace "prevent" with "reduce"

Response: Replaced

line 225: replace "must be limited to a mediujm size since" with "is a compromise between"

Response: Replaced

lines 245-247: The first sentence says sigma_n is estimate, the second sentence says that sigma_n = sigma_0 / 2. Which is it?

Response: We mean that the new background noise is estimated from the noise reduced data and the value is half of the original background noise.

line 297: replace "good" with "well"

Response: Replaced

line 301: remove "in nature"

Response: Removed.

line 331: remove "respectively"
Response: Removed

line 348-349: This isn't correct. There are many false clouds in the radar mask that don't correspond to large lidar backscatter.

Response: We modified this sentence as "This feature layer is also apparent in lidar observations with both relative large backscatter intensities and depolarization ratios**".**

line 364: remove "wispy-high-level"

Response: Removed.

line 395-396: remove first sentence here. Don't speculate on unpublished results.

Response: The sentence is removed.

Fig. 6e: add a zoom-in view on the cirrus like in Fig. 6b/c

Response: A zoom-in view on lidar data is added.

Response to Anonymous Referee #2

-The paper presented a new approach to improve cloud detection from Millimeter wavelength cloud radar measurements. The method has potentials. However, this paper didn't present enough evidence to demonstrate that the approach is really better. Thus, the paper needs significant improvements before accepting for publication.

Response: We thank the reviewer for his/her constructive comments and suggestions on this manuscript, which are very helpful for us to improve our paper. This paper is mainly a description of an improved hydrometeor detection approach for cloud radar. Additional work has been done and the results do show our method can recognize more signals. Our responses to the comments are given below.

- As illustrated in Fig. 6, the new method picks up more thin clouds detected by MPL (correctly), but it also picks up significant more clouds in the lower troposphere due tonoise. If this is the best case to illustrate the approach, it is hard to convince readers that the new approach is better.

Response: The increased detections in the lower troposphere are not due to noise. They could be some large dust particles. As shown in Fig 1, the depolarization ratio around 2 km is larger than surroundings. We also analyzed our radar Liner Depolarization Ratio (LDR) in Figure 2. It is clear that those increased detections around 2 km have large LDRs compared to that of noise. Although the dust is not desired information for cloud mask, the appearance of those particles and their detection prove the capability of our method on recognizing weak signals.

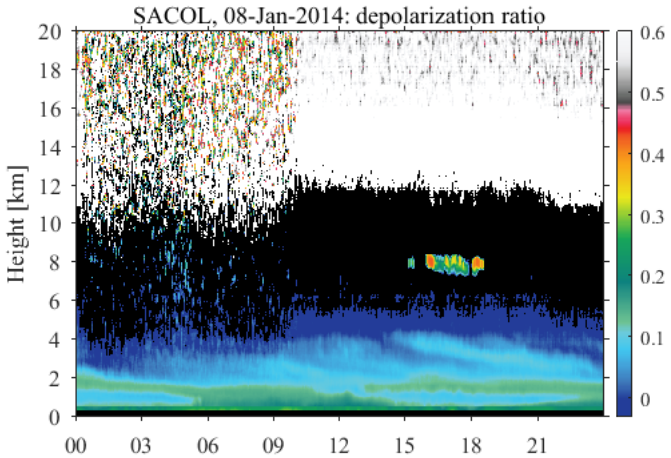

Figure 1. Depolarization ratio of MPL for January 8, 2014

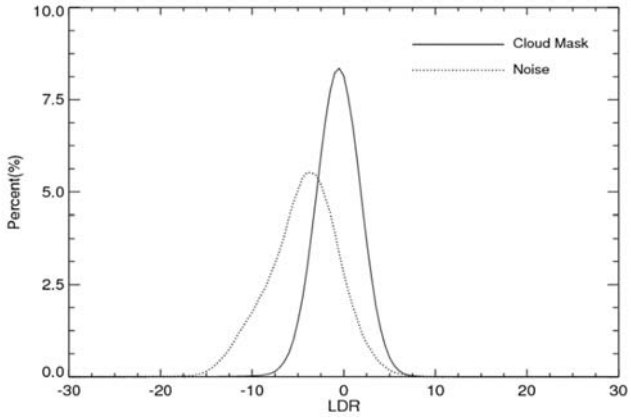

Figure 2. Radar LDR distributions for increased detections in the lower atmosphere and noise.

-Figure. 8 is a simple comparison between the two approaches; it is hard to demonstrate which one is more reliable. To show the new approach improving cloud detection for weak cloud signals, it is important to have lidar measurements as a truth for each cloud layer. Then you can provide quantitative assessments on improvements in both correct and false detections.

Response: We compare the radar cloud mask results derived from our method and ARM algorithm with the MPL detected features in January and July, 2014 when both radar and lidar observations are available. It is found that the increased detections by our method as compared with the ARM algorithm are mostly those also identified as features by MPL. Figure 3 shows an example in January 5, 2014. The features that are not observed by MPL are mainly related to a total attenuation of lidar signals by optically thick clouds below or appear at the base of clouds from where large hydrometeors may fall out which can not be observed by MPL.

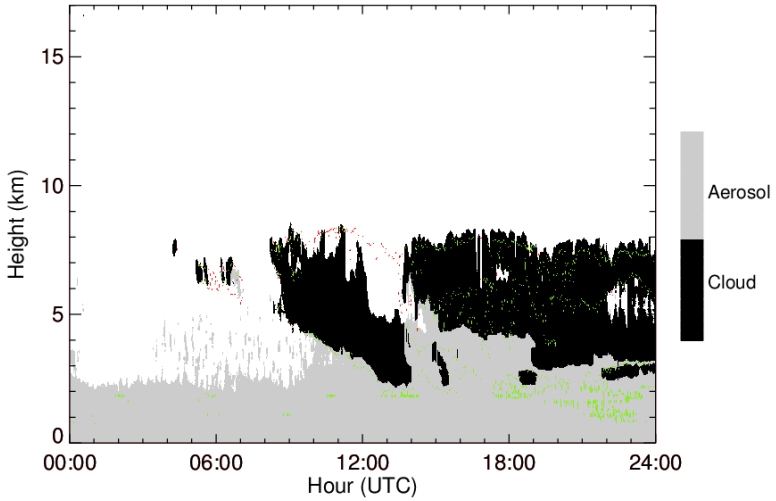

Figure 3. Increased hydrometeor detections by our algorithm versus ARM algorithm in comparison with the MPL feature mask in January 5, 2014. The black and gray regions represent the cloud and aerosol detected by MPL. The green part represents the

increased detections that are also identified as features by MPL detection. The red part represents the increased detection that are not detected by MPL.

We also calculated the percentage of the increased detections identified by both our mothed and MPL observations in the total increased detections only found by our mothed as shown in Figure 4. We can see that most part of the increased detection from our method is also detected as features by MPL. The percentage drops to a minimum of 70% at about 9 km, where the total increased cloud range bins are only about 110 and there are 35 range bins that are identified by our method are not observed by MPL. Considering all the increased detections by our method, 98.6% of them are confirmed by MPL as features.

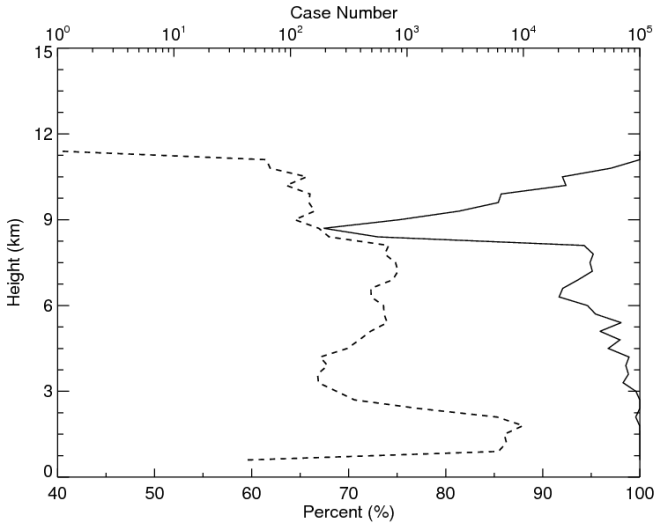

Figure 4. The solid line is the percentage of increased detections seen by both KAZR with our method and MPL as compared with the total increased detections. The dot line is the number of increased detections in each level.

-Although it is possible for cloud radar to detect dust storm when significant large dust particles were lifted in the atmosphere, such as dust storm illustrated in Auxiliary Figure1. But it is not possible to detect elevated thin dust layer because large dust particles fall out quickly after transporting certain distances. Thus, dust is not a possible explain for increased cloud detection by the new method at the low atmosphere in Fig. 6. Do you have depolarization measurements from your lidar? It will be great that you can provide depolarization measurements to further illustrate the occurrence of dust.

Response: Yes, we believe that long range transported dust particles should not be detected by millimeter radar. But as shown in Fig. 1, the large MPL depolarization ratio appear in the layer around 2 km. Figure 5 shows the MPL depolarization ratio for Januray 9, 2014. It can be seen that the increased detections in the lower atmosphere by our method in Fig. 3 correspond well with the large lidar depolarization.

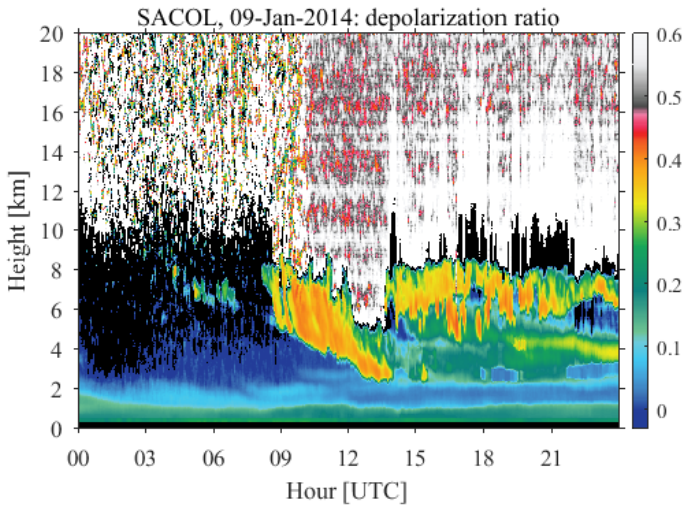

Figure 5. Depolarization ratio of MPL for January 9, 2014

-For the bottom two figures of Fig. 7: How is the percentage calculated, related to the total measurement profiles or other parameters? The high increasing region in the upper troposphere is corresponding to small case numbers. So an important question is what is the over all impacts on cloud amount. From cloud microphysics retrievals, what are potential impacts on upper troposphere cloud water content and radiative heating? Any justification for the importance of these missing clouds is helpful to justify the value of the new algorithm.

Response: The percentage is calculated by taking the ARM approach as a reference. The two lines represent the percentage of the increased detection by our method compared to ARM algorithm. Yes, it is true the high increasing region in the upper troposphere corresponds to small cloud amount. Small cloud amount should not be expected to have significant impacts on radiative heating. But these missing clouds may still be important for understanding the cloud formation and its relation to atmospheric conditions.

More importantly the optically thin cirrus clouds prevail in tropical upper troposphere. Applying our algorithm to cloud radar observations in the tropics would enhance the detection of thin cirrus there, which will be our future research.

-Many typos in the paper need to be corrected, for example, line 349, "evens" should be "events".

Response: We have corrected this error and carefully revised the manuscript again.

Response to Anonymous Referee #3

- In my view this paper is well-written, straightforward and makes a solid contribution to detection of atmospheric returns in radar receiver power outputs. Relative to the ARM algorithm (and perhaps the CloudSAT algorithm too?) it decreases the number of false negatives while importantly keeping the number of made up cloud detections (i.e., false positives) low in number as it must. I recommend its publication in Atmospheric Chemistry and Physics. I would like to see one addition to the paper which I outline below and then I have a few minor comments and clarifications that follow.

Response: We thank the reviewer for his/her constructive comments and suggestions on this manuscript, which are very helpful for us to improve our paper. Our responses to the reviewer's comments/suggestions are given below.

-On Line 343 the following sentence occurs: "This thin cirrus, however, is well-captured by our cloud mask method (Fig. 6b)." This is a subjective statement and I do not think that a comparison of Fig. 6b to Fig. 6e supports it. Comparison of Fig. 6b to Fig.6c shows improvement of the new algorithm relative to the ARM one, thereby lending support to the value of this new algorithm, but the thin cirrus appears to be much better detected by the lidar than the radar with application of either the proposed or ARM algorithms. Similarly, on Lines 378-380 the following sentence occurs: "This is because hydrometeors in the upper of troposphere are usually with smaller size and cause weak SNR values that will be effectively detected by the noise reduction scheme." The paper does demonstrate that the new algorithm does a better job detecting thin cirrus than the ARM algorithm but the paper does not demonstrate that thin cirrus "will be effectively detected by the noise reduction scheme." To address this weakness in the paper the authors should remove all subjective words from the paper, like "good", "well-captured", "remarkable" and replace them with comparative statistics. Morever, the authors state that they have mapped lidar and radar data to the same time height grid (see Lines 335-337. They should use this mapping to provide the percentage detected in Fig. 6b relative to Fig. 6e. Moreover, in a figure similar to Figure 7, the authors should illustrate results of the number of all lidar cloud detections also detected by the radar (but not necessarily vice versa as the goal is to determine how good the new algorithm is at mapping all lidar detected clouds) as a function of height. If this site had a lot of thin cirrus during either January or July 201, this will be a good test of the new algorithm applied to radar data. With these new results in the paper it will be interesting to see if the authors' claims on Lines 391-394 will hold up.

Response: We thank the reviewer for the insightful comments very much. We compare the radar cloud mask results derived from our method and ARM algorithm with the MPL detected features in January and July, 2014 when both radar and lidar observations are available. We calculated the percentage of the increased detections identified by both our mothed and MPL observations in the total increased detections only found by our mothed as shown in Figure 1. We can see that most part of the increased detection

from our method is also detected as features by MPL. The percentage drops to a minimum of 70% at about 9 km, where the total increased cloud range bins are only about 110 and there are 35 range bins that are identified by our method are not observed by MPL. Considering all the increased detections by our method, 98.6% of them are confirmed by MPL as features. We replaced the subjective words with comparative statistics in the revised manuscript.

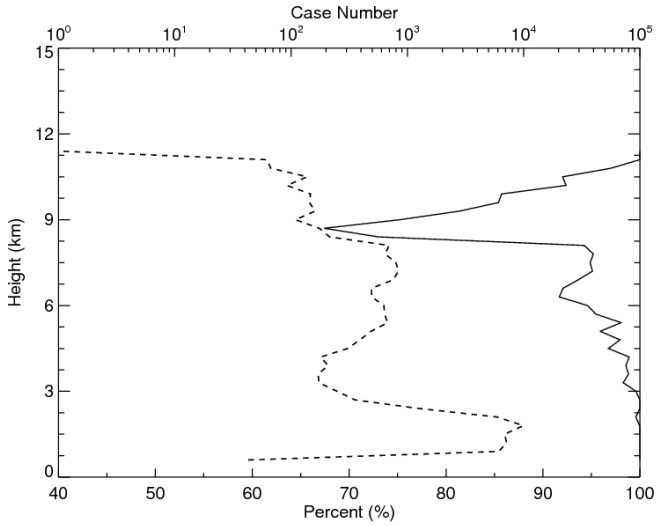

Figure 1. The solid line is the percentage of increased detections seen by both KAZR with our method and MPL as compared with the total increased detections. The dot line is the number of increased detections in each level.

Minor details:
1) Line 141: On this line a reference is made to "the noise power". Is this noise power just individual values of Pn from the top 30 range gates without being averaged? Please make it perfectly clear the source of the data for the non-Gaussian curve in Figure. 1a.

Response: We have added a reference to the noise power. The power distribution is derived from individual values of Pn at the top 30 range gates. The statement is clarified.

2) Lines 149-150: "SNRs for clear skies closely follow a Gaussian distribution" Lines 151-152: "SNR for the noise does not exactly obey the Gaussian distribution" For clear sky the SNRs represent noise, right? If so, these two phrases seem to contradict each other. Minimally, I do not understand what the authors are trying to say here.

Response: Yes, for clear sky the SNR values represent noise. The second phrase is used to explain the reason why the mean value of the SNR is not zero. We have modified this part in the revised manuscript to avoid confusions.

3) Line 176: I am not sure what "of each five successive profiles" means. Does this mean that the 150 range gate powers from the top 30 of five consecutive profiles are used to compute S_o and Sigma_o? Do these five profiles move with the 5 by 5

processing window that is used to create the results for this paper?

Response: Yes, it means the total 150 range gate powers from the top 30 of given five consecutive profiles and these five profiles move with the 5 by 5 spatial filter.

4) Line 275: "Note that a larger": Should "larger" be "smaller" here?

Response: We thank the reviewer for the careful review. Yes, it should be smaller here. “larger” is replaced with “smaller”.

5) Line 297: "detection method works quite good": Remove the words "quite good" and quantify what you mean.

Response: “quite good” is removed. We have modified the statement here.

An Improved Hydrometeor Detection Method for Millimeter-Wavelength Cloud Radar

Ge Jinming[1], Zhu Zeen[1], Zheng Chuang[1], Xie Hailing[1], Zhou Tian[1], Huang Jianping[1], and Fu Qiang [1,2]

[1]Key Laboratory for Semi-Arid Climate Change of the Ministry of Education and College of Atmospheric Sciences, Lanzhou University, Lanzhou, 730000, PRC

[2]Department of Atmospheric Sciences, University of Washington, Seattle, WA, 98105, USA

December, 2016

Abstract

A new method is proposed to distinguish clouds and other hydrometeors from noise in cloud radar observations. A noise reduction scheme that can reduce the noise distribution to a narrow range is proposed in our method in order to recognize more weak signal clouds. A spatial filter with central weighting, which is used in current cloud radar hydrometeor detection algorithms, is also involved in our method to ~~Instead of examining~~ examine radar return for significant levels of signals., ~~which is used in current cloud radar hydrometeor detection algorithms, this new method extracts signals by first reducing noise distribution to a narrow range.~~ "Square clouds" were constructed to test the two schemes. We applied our method to ~~two~~ six months of cloud radar observations~~,~~ and compared the results with those obtained by applying the U.S. Department of Energy (DOE) Atmospheric Radiation Measurements (ARM) program operational algorithm. It was found that our method has significant advantages in recognizing clouds with weak signal and reducing the rates of both failed negative and false positive hydrometeor identifications in simulated clouds.

1. Introduction

Clouds, which are composed of liquid water droplets, ice crystals or both, ~~move around our planet and~~ cover about two-thirds of the earth surface at any time [e.g., *King et al.*, 2013]. By reflecting solar radiation back to the space (the albedo effect) and trapping thermal radiation emitted by the Earth surface and the lower troposphere (the greenhouse effect), clouds strongly modulate the radiative energy budget in the climate system [e.g., *Fu et al.*, 2002; *Huang et al.*, 2007; *Huang et al.*, 2006a; *Huang et al.*, 2006b; *Ramanathan et al.*, 1989; *Su et al.*, 2008]. Clouds are also a vital ~~stage~~ component of water cycle by connecting the water-vapor condensation and precipitation. Despite the importance of clouds in the climate system, they ~~cannot~~ are difficult to~~be accurately~~ represent~~ed~~ in climate models [*Williams and Webb*, 2009], which causes the largest uncertainty in the predictions of climate change by general circulation models (GCMs) [e.g., *Randall*, 2007; *Stephens*, 2005; *Williams and Webb*, 2009].

Cloud formation, evolution and distribution are governed by complex physical and dynamical processes on a wide range of scales from synoptic motions to turbulence [*Bony et al.*, 2015]. Unfortunately, the processes that occur on smaller spatial scales than a GCM grid box cannot be resolved by current climate models, and the coupling between large scale fluctuations and cloud microphysical processes are not well understood [e.g., *Huang et al.*, 2006b; *Mace et al.*, 1998; *Yan et al.*, 2015; *Yuan et al.*, 2006]. Moreover, the cloud horizontal inhomogeneity and vertical overlap are not resolved by GCMs [*Barker*, 2000; *Barker and Fu*, 2000; *Fu et al.*, 2000a; *Fu et al.*,

2000b; *Huang et al.*, 2005; *Li et al.*, 2015]. To better understand cloud processes for improving their parameterization in climate models and revealing their evolution in response to climate change, long-term continuous observations of cloud fields in terms of both macro- and micro-physical properties are essential [e.g., *Ackerman and Stokes*, 2003; *Sassen and Benson*, 2001; *Thorsen et al.*, 2011; *Wang and Sassen*, 2001].

Millimeter-wavelength Cloud Radars (MMCRs) ~~are powerful instruments that~~ can resolve cloud vertical structure for their occurrences and microphysical properties [e.g., *Clothiaux et al.*, 1995; *Kollias et al.*, 2007a; *Mace et al.*, 2001]. The wavelengths of MMCRs are shorter than those of weather radars ~~and they have excellent~~making them sensitivity to cloud droplets and ice crystals and can penetrate multiple cloud layers [e.g., *Kollias et al.*, 2007a]. Because of their outstanding advantages for cloud research, millimeter-wavelength radars have been deployed on various research platforms including the first space-borne millimeter-wavelength Cloud Profiling Radar (CPR) onboard the CloudSat [*Stephens et al.*, 2002]. Ground-based cloud radar ~~MMCRs~~ are operated ~~in~~ at the U.S. Department of Energy's Atmospheric Radiation Program (ARM) observational sites (used to MMCRs, now are replaced with a new generation of Ka band Zenith Radar (KAZR)) [e.g., *Ackerman and Stokes*, 2003; *Clothiaux et al.*, 2000; *Clothiaux et al.*, 1999; *Kollias et al.*, 2007b; *Protat et al.*, 2011] and in Europe [*Illingworth et al.*, 2007; *Protat et al.*, 2009]. In July 2013, ~~a new generation of Ka band Zenith Radar (KAZR)~~ KAZR was deployed in China at the Semi-Arid Climate and Environment Observatory of Lanzhou University (SACOL) site (latitude: 35.946°N; longitude: 104.137°E; altitude: 1.97 km) [*Huang et al.*, 2008], providing an

opportunity to observe and reveal the detailed structure of the mid-latitude clouds over East Asia semi-arid regions.

Before characterizing the cloud physical properties from the cloud radar return signal, we first need to distinguish and extract the hydrometeor signals from the background noise (i.e. cloud mask). A classical cloud mask method was developed in Clothiaux et al.[2000; 1995] by analyzing the strength and significance of returned signals. This method consists of two main steps. First any power in a range gate that is greater than a mean value of noise plus one standard deviation is selected as a bin containing potential hydrometer signal. Second, a spatial-time coherent filter is created to estimate the significance level of the potential hydrometer bin signal to be real. This cloud mask algorithm is operationally used for the ARM MMCRs data analysis and was later ~~successfully modified and~~ adopted to the CPR onboard the CloudSat [*Marchand et al.*, 2008].

It is recognized that by visually examining a cloud radar return image, one can easily tell where the return power is likely to be caused by hydrometeors and where the power is just from noise. This ability of human eye on extracting and analyzing information from an image has been broadly studied in image processing and computer vision, and a number of mathematical methods for acquiring and processing information from images have been developed, including some novel algorithms for noise reduction and edge detection [*Canny*, 1986; *He et al.*, 2013; *Marr and Hildreth*, 1980; *Perona and Malik*, 1990]. In this paper we develop a new cloud mask method for cloud radar by noticing that removing noise from signal and identifying cloud boundaries are the

104 essential goals of cloud mask. This method reduces the radar noise while preserving
105 cloud edges by employing the bilateral filtering that is widely used in the image
106 processing [*Tomasi and Manduchi*, 1998]. The power weighting probability method
107 proposed by Marchand et al.[2008] is also adopted in our method to prevent the cloud
108 corners from being removed. It is found that our improved hydrometeor detection
109 algorithm is more efficient in terms of reducing false positives and negatives as well as
110 identifying cloud features with weak signals such as thin cirrus clouds.

111 The KAZR deployed at the SACOL is described in section 2 and the new cloud mask
112 algorithm is introduced in section 3. The applications of the new scheme to both
113 hypothetical and observed cloud fields including a comparison with previous schemes
114 are shown in section 4. Summary and conclusions are given in section 5.

115 2. The KAZR Radar

116 The SACOL KAZR, built by ProSensing Inc. of Amherst, MA, is a zenith-pointing
117 cloud radar operating at approximately 35 GHz for the dual-polarization measurements
118 of Doppler spectra. The main purpose of the KAZR is to provide vertical profiles of
119 clouds by measuring the first three Doppler moments: reflectivity, radial Doppler
120 velocity, and spectra width. The linear depolarization ratio [*Marr and Hildreth*, 1980]
121 can be computed from the ratio of cross-polarized reflectivity to co-polarized
122 reflectivity.

123 The SACOL KAZR has a transmitter with a peak power of 2.2 kw and two modes
124 working at separate frequencies. One is called “chirp” mode that uses a linear-FM
125 (frequency modulation) pulse compression to achieve high radar sensitivity of about -

65 dBZ at 5 km altitude. The minimum altitude (or range) that can be detected in chirp mode is approximately 1 km AGL. To view clouds below 1 km, a short pulse or "burst mode" pulse is transmitted at a separate frequency just after transmission of the chirp pulse. This burst mode pulse allows clouds as low as 200 m to be measured. The chirp pulse is transmitted at 34.890 GHz while the burst pulse is transmitted at 34.830 GHz. These two waveforms are separated in the receiver and processed separately.

The pulse length is approximately 300 ns (giving a range resolution of 45 m), while the digital receiver samples the return signal every 30 m. The interpulse period is 208.8 μs, the number of coherent averages is 1, and the number of the fast Fourier transform (FFT) points is currently set to 512. An unambiguous range is thus 31.29 km, an unambiguous velocity is 10.29 m/s, and a velocity resolution of is 0.04m/s. The signal dwell time is 4.27s. These operational parameters are set for the purpose of having enough radar sensitivity and accurately acquiring reflectivities of hydrometeors. In this study, we mainly use radar observed reflectivity (dBZ) data to test our new hydrometeor detection method.

3. Hydrometeor detection algorithm

The basic assumption in the former cloud mask algorithms [*Clothiaux et al.*, 1995; *Marchand et al.*, 2008] is that the random noise power follows the normal distribution. In this study, several clear sky cases in all seasons from the KAZR observations were firstly selected to analyze its background noise power distributions (Fig.1). ~~However,~~ As demonstrated in Fig.1a for a clear-sky case during 0000 to 1200 UTC on January 21st, 2014, the noise power estimated from the top 30 range gates, which includes both

internal and external sources[*Fukao and Hamazu*, 2014], has an apparent non-Gaussian distribution with a positive skewness of 1.40. The signal-to-noise ratio (SNR) is defined as:

$$\mathrm{SNR} = 10\log\left(\frac{P_s}{P_n}\right) \quad (1)$$

where P_s is the power received at each range gate in a profile, P_n is the mean noise power that is estimated by averaging the return power in the top 30 range gates which are between 16.8 and 17.7 km AGL. Since this layer is well above the tropopause, few atmospheric hydrometeors existing in this layer can scatter enough power back to achieve the radar sensitivity. Figure 1a shows that the SNRs for clear skies closely follow a Gaussian distribution. Instead of using radar received power, the SNR is used to estimate the background noise level and taken as the input to the cloud mask procedure since~~.~~ the SNR satisfies the assumption of a normally distributed noise and in our method the chance for the central range gate to be a noise or a potential signal relies on calculating the probability for a given range of SNR values based on the Gaussian distribution. Note that the mean value of the SNR for the noise power is not zero, but a small negative value of about -0.3. This is because the mean of the noise power is larger than its the median due to its positive skewed distribution~~SNR for the noise does not exactly obey the Gaussian distribution~~. It is further noted that the distribution of SNR and its mean for the top 30 range gates are the same as those from the lower atmosphere.

The SNR value is treated as the brightness of a pixel in an image $f(x, y)$ in our hydrometeor detection method. In an image processing, the random~~ly Gaussian~~

~~distributed~~ noise can be smoothed out by using a low pass filter, which gives a new value for a pixel of an image by averaging with neighboring pixels [*Tomasi and Manduchi*, 1998]. The cloud signals are highly correlated in both space and time and have more similar values in near pixels while the random noise values are not correlated. Therefore, as illustrated in Fig. 2a, this low pass filter can efficiently reduce the original radar noise represented by the green line to a narrow bandwidth (blue line) while keeping the signal preserved. By reducing the standard deviations of noise, which shrinks the overlap region of signal and noise and enhances their contrast, the weak signals (yellow area) that cannot be detected based on original noise level may become distinguished.

Based on this idea, we develop a non-iterative hydrometeor detection algorithm by applying a noise reduction and a central pixel weighting schemes. Figure 3 shows the schematic flow diagram of our method. The input SNR data set is first separated into two groups. One group with values greater than the mean background noise SNR (S_o) plus three times of its standard deviation (σ_o) are considered as the cloud features that can be confidently identified. Another group with values between S_o and $S_o + 3\sigma_o$ may potentially contain moderate ($S_o + \sigma_o < SNR \leq S_o + 3\sigma_o$) to weak ($S_o < SNR \leq S_o + \sigma_o$) cloud signals, which will further go through a noise reduction process. Here S_o and σ_o are estimated from the top 30 range gates of each five successive profiles.

The noise reduction process is mainly performed by convolving radar SNR time-height data with a low pass filter. The Gaussian Filter, which outputs a `weighted average' of each pixel and its neighborhood with the average weighted more towards

192 the value of the central pixel (v_0), is one of the most common functions of the noise
193 reduction filter. A 2-D Gaussian distribution kernel, shown in Fig. 2b1, can be expressed
194 as:

195 $$G(i,j) = \frac{1}{2\pi\sigma^2}\exp(-\frac{i^2+j^2}{2\sigma^2}) \quad (2)$$

196 where i and j are the indexes in a filter window which are 0 for the central pixel, and σ
197 is standard deviation of the Gaussian distribution for the window size of the kernel.
198 Equation (2) is used in our study to filter the radar SNR image. Note that the
199 convolution kernel is truncated at about three standard deviations away from the mean
200 in order to accurately represent the Gaussian distribution. Figure 1b are the cumulative
201 distribution functions (CDFs) of clear sky SNR by convolving the same data in Fig. 1a
202 with four filters that have different kernel sizes (3×3, 5×5, 7×7 and 9×9 pixels)
203 corresponding to the σ ranging from 0.5 to 2. The original SNR values are distributed
204 from about -5 to 5. After convolving the image with the Gaussian filter, the SNR
205 distribution can be constrained to a much narrower range. It is clear that the filter with
206 a larger kernel size is more effective in suppressing the noise. Shown in Fig. 1c are
207 results for a cloudy case on January 4th,2014 by applying the filter to the range gates
208 inside the cloud but adjacent to the boundary, showing that a larger kernel size shifts
209 the SNR farther away from the noise region. It therefore appears that increasing the
210 standard deviation (i.e. the window size) continues reducing the noise and increasing
211 the contrast between signal and noise more effectively. On the other hand, a larger
212 kernel can also attenuate or blur the high frequency components of an image (e.g., the
213 boundary of clouds) more at the same time. As shown in Fig. 1d, when the window size

is increased from 3×3 (σ=0.5) to 9×9 (σ=2), the SNR distribution of the range gates that are outside the cloud but adjacent to the boundary gradually move toward larges values. This will consequently raise the risk of misidentifying cloud boundaries. To solve this problem, a bilateral filtering idea proposed by *Tomasi and Manduchi* [1998] is adopted here. Considering a sharp edge between cloudy and clear region as shown in Fig. 2b$_2$, we define a $\delta(i,j)$ function that when the central pixel is on the cloudy or clear side, gives a weighting of 1 to the similar neighboring pixels (i.e. on the same side), and 0 to the other side. After combining this δ function to the Gaussian kernel in Fig. 2b$_1$, we can get a new non-linear function called bilateral kernel as shown in Fig. 2b$_3$. It can be written as:

$$\mathrm{B}(i,j) = \frac{1}{2\pi\sigma^2}\exp\left(-\frac{i^2+j^2}{2\sigma^2}\right)\cdot\delta(i,j). \qquad (3)$$

Thus the bilateral kernel will ~~prevent~~ reduce averaging noises with signals, and vice versa. The noise-reduced image $\mathrm{h}(\mathrm{x},\mathrm{y})$ is produced by convolving the bilateral kernel with the input image $f(\mathrm{x},\mathrm{y})$ as:

$$\mathrm{h}(x,y) = \mathrm{k}^{-1}(x,y)\sum_{j=-w}^{j=w}\sum_{i=-w}^{i=w} f(x+i,y+j)\cdot B(i,j) \qquad (4)$$

where ±w is the bounds of the finite filter window, $\mathrm{k}^{-1}(x,y)$ is defined as $1/\sum_{j=-w}^{j=w}\sum_{i=-w}^{i=w} B(i,j)$ which is used to normalize the weighting coefficients. Since the bilateral kernel function only average the central pixel with neighbors on the same side (Fig. 2b), ideally it will preserve sharp edges of a target. We will discuss how to construct the δ function in order to group the central pixel with its neighbors later in this section. In the noise reduction process, a 5×5 window size (i.e., 25 bins in total) is specified for the low pass filter, which is empirically determined by visually comparing

the cloud masks with original images. We should keep in mind that the window size is compromised ~~must be limited to a medium size~~ since a small window size is less effective in noise reduction but a large window is not suitable for recognizing weak signals.

For performing the noise reduction with Eq. (4) in a 5x5 filter window, the number of range bins (*Ns*) with signal greater than $S_o + 3\sigma_o$ are first counted. These N_s range bins are then subtracted from the total 25 of the range bins in the filter window. Note that a noise reduction is only applied when the central pixel is among the 25-Ns bins, and the δ function is set to be zero for the Ns range bins. If the remaining 25-N_s range bins are all noises, the range bin number (N_m) with SNR greater than $S_o + \sigma_o$ should be about equal to an integral number (N_t) of 0.16×(25-N_s) where 0.16 is the probability for a remaining range bin to have a value greater than $S_o + \sigma_o$ for a Gaussian noise. Thus when N_m is equal to or smaller than N_t, all the 25-N_s range bins could only contain pure noise and/or some weak cloud signals. In this case, the δ function is set to 1 for all the 25-N_s bins. When N_m is found to be larger than N_t, the 25-N_s range bins might contain a combination of moderate signal, noise and/or some weak clouds. In this case, $S_o + \sigma_o$ is selected as a threshold to determine whether the neighboring pixels are on the same side of the central pixel. If the central pixel has a value greater than $S_o + \sigma_o$, the δ function is assigned to 1 for the 25-N_s pixels with SNR $\geq S_o + \sigma_o$, but 0 for the neighboring bins with SNR $< S_o + \sigma_o$. If the central pixel is less than $S_o + \sigma_o$, the δ function is assigned to 1 for the neighboring pixels with SNR $< S_o + \sigma_o$, but 0 for the 25-Ns bins with SNR $\geq S_o + \sigma_o$.

After picking out the strong return signals and applying the noise reduction scheme, the new background noise S_n and its standard deviation σ_n are estimated. While S_n is the same as S_o, the σ_n is significantly reduced, which is a half of σ_o. This will make it possible to identify more hydrometeors as exhibited in Fig.2a. We assign different confidence level values to the following initial cloud mask according to the SNR. 40 is first assigned to the mask of any range bins with $SNR > S_o + 3\sigma_o$ in the original input data. For the rest of the range bins after applying the noise reduction, if the $SNR > S_n + 3\sigma_n$, the mask is assigned to be 30; if $S_n + 2\sigma_n < SNR \leq S_n + 3\sigma_n$, the mask is 20; if $S_n + \sigma_n < SNR \leq S_n + 2\sigma_n$, the mask is 10; and the remaining range bin mask is assigned to be 0.

To reduce both false positives (i.e. false detections) and false negatives (i.e. failed detections), the next step is to estimate whether a range gate contains significant hydrometeor. Following Clothiaux et al.[2000; 1995] and Marchand et al.[2008], a 5×5 spatial filter is used to calculate the probability of clouds and noise occurring in the 25 range gates. The probability of central pixel weighting scheme proposed by Marchand et al. [2008] is adopted, and the weighting for the central pixel is assigned according to its initial mask value. The probability is calculated by

$$p = G(L)(0.16^{N_T})(0.84^{N_0}) \quad (5)$$

where N_0 is the number of masks with zeros values, N_T is the number of masks with non-zeros values and $N_0 + N_T = 25$; G(L) is the weighting probability of the central pixel that could be a false detection where L is the significant level in the initial cloud mask [G(0)=0.84, G(10)=0.16, G(20)=0.028, G($\geqslant$30)=0.002]. If p estimated from Eq.

(5) is less than a given threshold (p_{thresh}), then the central pixel is likely to be a hydrometeor signal. The value in the cloud mask will set to be the same value as in the initial mask if it is non-zero; otherwise it will be set to 10. Likewise, if $p > p_{thresh}$, then the central pixel is likely to be noise and will be set to 0. This process is iterated 5 times for each pixel to obtain the final cloud mask.

Following Marchand et al. [2008] who well explained the logic of choosing a proper threshold, p_{thresh} is calculated as

$$p_{thresh} = (0.16^{N_{thresh}})(0.84^{25-N_{thresh}}) \quad (6)$$

Note that a ~~larger~~ smaller p_{thresh} will keep the false positives lower but increase the false negative. Herein the p_{thresh} of 5.0×10^{-12} used in Clothiaux et al.[2000], which is approximately equivalent to $N_{thresh} = 13$, is selected.

Figure 4 illustrate the main steps of ~~is a case to illustrate the steps of~~ our detection method by using the data from January 8th, 2014. Figure 4a is the original SNR input. Figure 4b shows the SNR distribution after the noise reduction process. ~~We~~One can see that the SNR is compressed to a narrow range and become ~~distribution of SNR is~~ much smoother than original input after the noise reduction process. This step significantly increases the contrast between signal and noise. ~~Fig. 4a.~~ Figure 4c indicates the range gates that potentially contain hydrometeors in the initial cloud mask. ~~. 4c and~~ Figure 4d is ~~are~~ the final result~~s~~ by applying the ~~binary mask and using a~~ spatial filter~~, respectively~~.

4. Results

4.1 Detection test

To test the performance of our hydrometeor detection method, we create 7 squares

of SNR with sides of 100, 50, 25, 15, 10, 5, and 3 bins to mimic the radar "time-height" observations as shown in Fig. 4~~5~~. The background noise is randomly given by a Gaussian distribution with a mean S_0 and a standard deviation σ_0. The targets in panels a_1, a_2 and a_3 are set with different SNR values to represent situations in which clouds have strong, moderate and weak signals, respectively. In panel a_1, the targets signals are set to be $S_0 + 10\sigma_0$. In panel a_2, the targets signals distribute from $S_0 + \sigma_0$ to $S_0 + 3\sigma_0$ with a mean value of $S_0 + 2\sigma_0$. In panel a_3, the targets SNRs range from S_0 to $S_0 + \sigma_0$ with a mean value of $S_0 + 0.5\sigma_0$.

The three middle panels in Fig. 4~~-~~5 show the results after applying the noise reduction. Comparing with the input signals, we can see that the background noise is well compressed and becomes more smooth. The shapes of the square targets are all well maintained with sharp boundaries for strong and moderate signals (see panels b1 and b2). In panel b_3 for weak signals, the 3-bin square target is not obvious while the other 6 squares are still distinguishable. To separate the compressed background noise from hydrometeor signals, the 5×5 spatial filter is further applied to the noise-reduced data. The three right panels in Fig.4~~-~~5 show the final mask results. Generally, the hydrometeor detection method ~~works~~ can identify those targets ~~quite good~~well. Six of the seven square targets can be identified for clouds with strong and moderate SNR. The 3×3 square is missed because the small targets cannot be resolved by the 5×5 spatial filter. Since the temporal resolution of KAZR is about 4 seconds, we expect that a cloud only having 3 bins in horizontal would be rare~~ in nature~~. For the targets with weak SNR values, the 3×3 and 5×5 square targets are missed, but the rest five square targets are

successfully distinguished and their boundaries are well maintained.

To further demonstrate the performance of our method to detect the hypothetical clouds in Fig.54 a1, a2, and a3, the false and failed detection rates are listed in the table 1. For strong signals, no background noise pixel is misidentified as one containing hydrometeors at level 40. Although at levels less than 40, some noise pixels around the edges of targets are identified as signals, the false detection is within 0.05%. The failed detection rate is about 0.24%. For moderate signals, the failed detection rate is still as small as 0.23%, while the false detection increases a little to 0.10% at the confidence levels below 30. The failed detection can reach up to 9.77% for weak signal at level 10, but more than 90% weak signals can be captured in our method. Note that the false positive is less than 0.01%; in other words, any range gate that is detected likely as a signal bin will have extremely high likelihood to contain hydrometeors.

The simple square clouds are also tested by using the ARM operational hydrometeor detection algorithm that does not include the noise reduction and weighting schemes. As can be seen in Fig. 65, the ARM operational algorithm can only find five of the seven square targets with strong and moderate SNR. Meanwhile without central pixel weighting, the corners of the targets become rounded and more than 2.23% of hydrometeors are missed for strong and moderate cloud cases. Without the noise reduction, none of the weak cloud signals can be detected. Comparing Fig.4–5 and Fig.56, it is obvious that our hydrometeor detection method can well maintain the cloud boundary, keep both false and failed detection rate as low as a few percent for strong and moderate cloud cases, and has a remarkable advantage in recognizing weak signals.

4.2 Application to the SACOL KAZR observations

Our hydrometeor detection method was then applied to ~~one~~the winter and ~~one~~ summer months (Dec. in 2013, Jan., Feb., Jun., Jul. and Aug. in 2014) KAZR data at the SACOL. A micropulse lidar (MPL) transmitted at 527 nm is operated nearby the KAZR. Lidar is more sensitive to thin cirrus clouds and thus used to assess the performance of our algorithm. Figures 7~~6~~ a, b and c show an one-day example of radar reflectivity, normalized backscatter and depolarization ratio of lidar, respectively. The cloud masks from our detection method and the ARM operational method without the noise reduction and the central pixel weighting are shown in Fig. 7d&e. The ~~compared with~~ MPL feature mask ~~by MPL~~ derived by modifying the method ~~in~~proposed in Thorsen et al. [2015] and Thorsen and Fu [2015] ~~which are~~is shown in Fig. 7f. The vertical and horizontal resolutions of the radar and lidar are different, and we map the observed data and derived feature mask on the same height and time coordinates for a simple comparison. A distinct thin feature layer appears at about 8 km during 1500 to 1830 UTC form the lidar observation which is clearly identified as a cirrus cloud using the depolarization ratio. The contrast between the cirrus layer and background from the KAZR observation (Fig. 7~~6~~a) is very weak, and only a few range gates are identified as the ones containing hydrometeors using the method without the noise reduction and weighting (Fig. 7~~6~~d~~c~~). However, our cloud mask method can find more range gates (about 2.8 times of ARM's result). All these increased range bins from our method are also detected as~~This~~ thin cirrus by the MPL~~, however, is well captured by our cloud mask method~~ (Fig. ~~6b~~7f). Another apparent discrepancy exists in the low

atmosphere layer. A non-negligible number of range gates at about 2 km are recognized as hydrometeor echoes by our method but mostly missed by former technique. This feature layer is also apparent in lidar observations with both relative large backscatter intensities and depolarization ratios(Fig. 7b & c). MPL recognizes this feature as an aerosol layer. In our KAZR observations, we did find some dust events ~~evens~~ that were detected by this millimeter wavelength radar (see the auxiliary Fig.1). Those hydrometeor echoes detected by our method might partly be caused by large dust particles. Although the dust is not desired for cloud mask, the appearance of those particles dose prove the ability of our method on recognizing weak signals.

The upper two panels in Fig. 8 compares the number of occurrences of the detected hydrometeor range bins from our new methods with that from the ARM operational algorithm for the six months– of data. Generally, one can see that the variations of the identified hydrometeor numbers with height from the two techniques are in a good agreement. The distinct discrepancies appear at about 2 km in Winter~~January~~ and above 13 km in Summer~~July~~ where our method apparently identify more hydrometeors. To illustrate the improvements of our method and quantitatively evaluate the two schemes used in the algorithm, we plot the percent change of the detected hydrometeor bins form our method comparing with that from the ARM operational method in the lower two panels in Fig. 8~~7~~. As expected from the results in the test square clouds, our method can identify more signals. The remarkable feature is that the increased percentage is over 20% at high altitude, indicating that our method can recognize more ~~wispy high-level~~ cirrus clouds. The increased percentage of hydrometeor derived only with the

weighting scheme (dashed line) and with both the noise reduction and weighting schemes (solid line) are separated to demonstrates the individual contribution of the scheme to the improvement of our method. In winter ~~January~~, the number of the detected hydrometeors only with the weighting scheme is almost the same as that from the ARM operational method at layer from 3.5 to 9 km AGL, while this number will increase by about 5% if the noise reduction scheme is involved, indicating that some hydrometeors with weak SNR values may exit in this layer. Above and below this atmospheric layer, the increased percentage is largely determined by the weighting scheme. In summer~~July~~, the two line almost overlap each other between 3.5 and 9.5 km with values below 5%, revealing that the bins found by our method in the middle atmospheric layer are mainly around the boundaries of clouds. We may infer that in summer season, clouds in middle level are usually composed of large droplets with strong SNR values. The two lines are gradually apart with height. This is because hydrometeors in the upper of troposphere are usually with smaller size and cause weak SNR values that will be effectively detected by the noise reduction scheme. Note that the confusion matrix shows that the cancellation errors can be negligible.

We also analyzed data in January July, 2014 when both KAZR and MPL observations are available, and showed the percentage of the increased detections identified by both KAZR with our method and MPL observations as compared to the total increased detections in Fig. 9. It is obviously that most of the increased detections are also detected as features by MPL. The percentage drops to a minimum of 70% at about 9 km, where the total increased cloud range bins are only about 110 and there are 35 range

bins that are identified by our method not observed by MPL. Considering all the increased detections by our method, 98.6% of them are confirmed by MPL as features.

5. Summary and Discussion

Based on image noise reduction technique, we propose a new method to detect hydrometeors from cloud radar return signals. The basic idea is to treat the SNR value of each range gate as a pixel brightness and suppress the SNR distributions of noise to a narrow range by convolving with a 2-D bilateral kernel. After the noise smoothing process, a special filter with central-pixel weighting scheme is used to get the final cloud mask. The test square clouds show that there are two remarkable advantages of our method: First the noise reduction scheme of our algorithm can enhance the contrast between signal and noise, while keeping the cloud boundaries preserved and detecting more hydrometeors with weak SNR values. Second both false positive and failed negative rates for strong and moderate clouds can be reduced to acceptably small values. A comparison of radar and lidar observed case further highlight the advantage of our method in application.

~~Note that CloudSat cloud mask may have a large false detection for weak echoes. We are actively working to apply our new detection method to CloudSat observations.~~

Acknowledgements: This work was supported by the National Science Foundation of China (41430425, 41575016, 41521004, 41505011), China 111 project (No.B 13045), and the Fundamental Research Funds for the Central University (lzujbky-2016-k01).

Reference

Ackerman, T. P., and G. M. Stokes (2003), The Atmospheric Radiation Measurement program (vol 56, pg 38, 2003), *Physics Today*, *56*(2), 14-14.

Barker, H. W. (2000), Indirect aerosol forcing by homogeneous and inhomogeneous clouds, *Journal of Climate*, *13*(22), 4042-4049, doi:10.1175/1520-0442(2000)013<4042:iafbha>2.0.co;2.

Barker, H. W., and Q. Fu (2000), Assessment and optimization of the gamma-weighted two-stream approximation, *Journal of the Atmospheric Sciences*, *57*(8), 1181-1188, doi:10.1175/1520-0469(2000)057<1181:aaootg>2.0.co;2.

Bony, S., et al. (2015), Clouds, circulation and climate sensitivity, *Nature Geoscience*, *8*(4), 261-268, doi:10.1038/ngeo2398.

Canny, J. (1986), A COMPUTATIONAL APPROACH TO EDGE-DETECTION, *Ieee Transactions on Pattern Analysis and Machine Intelligence*, *8*(6), 679-698.

Clothiaux, E. E., T. P. Ackerman, G. G. Mace, K. P. Moran, R. T. Marchand, M. A. Miller, and B. E. Martner (2000), Objective determination of cloud heights and radar reflectivities using a combination of active remote sensors at the ARM CART sites, *Journal of Applied Meteorology*, *39*(5), 645-665, doi:10.1175/1520-0450(2000)039<0645:odocha>2.0.co;2.

Clothiaux, E. E., M. A. Miller, B. A. Albrecht, T. P. Ackerman, J. Verlinde, D. M. Babb, R. M. Peters, and W. J. Syrett (1995), AN EVALUATION OF A 94-GHZ RADAR FOR REMOTE-SENSING OF CLOUD PROPERTIES, *Journal of Atmospheric and Oceanic Technology*, *12*(2), 201-229, doi:10.1175/1520-0426(1995)012<0201:aeoagr>2.0.co;2.

Clothiaux, E. E., K. P. Moran, B. E. Martner, T. P. Ackerman, G. G. Mace, T. Uttal, J. H. Mather, K. B. Widener, M. A. Miller, and D. J. Rodriguez (1999), The atmospheric radiation measurement program

cloud radars: Operational modes, *Journal of Atmospheric and Oceanic Technology*, *16*(7), 819-827, doi:10.1175/1520-0426(1999)016<0819:tarmpc>2.0.co;2.

Fu, Q., M. Baker, and D. L. Hartmann (2002), Tropical cirrus and water vapor: an effective Earth infrared iris feedback?, *Atmospheric Chemistry and Physics*, *2*, 31-37.

Fu, Q., B. Carlin, and G. Mace (2000a), Cirrus horizontal inhomogeneity and OLR bias, *Geophysical Research Letters*, *27*(20), 3341-3344, doi:10.1029/2000gl011944.

Fu, Q., M. C. Cribb, and H. W. Barker (2000b), Cloud geometry effects on atmospheric solar absorption, *Journal of the Atmospheric Sciences*, *57*(8), 1156-1168.

Fukao, S., and K. Hamazu (2014), Radar for Meteorological and Atmospheric Observations, *Springer*.

He, K., J. Sun, and X. Tang (2013), Guided Image Filtering, *Ieee Transactions on Pattern Analysis and Machine Intelligence*, *35*(6), 1397-1409, doi:10.1109/tpami.2012.213.

Huang, J. P., J. Ge, and F. Weng (2007), Detection of Asia dust storms using multisensor satellite measurements, *Remote Sensing of Environment*, *110*(2), 186-191, doi:10.1016/j.rse.2007.02.022.

Huang, J. P., P. Minnis, B. Lin, Y. H. Yi, T. F. Fan, S. Sun-Mack, and J. K. Ayers (2006a), Determination of ice water path in ice-over-water cloud systems using combined MODIS and AMSR-E measurements, *Geophysical Research Letters*, *33*(21), doi:10.1029/2006gl027038.

Huang, J. P., P. Minnis, B. Lin, Y. H. Yi, M. M. Khaiyer, R. F. Arduini, A. Fan, and G. G. Mace (2005), Advanced retrievals of multilayered cloud properties using multispectral measurements, *Journal of Geophysical Research-Atmospheres*, *110*(D15), doi:10.1029/2004jd005101.

Huang, J. P., Y. J. Wang, T. H. Wang, and Y. H. Yi (2006b), Dusty cloud radiative forcing derived from satellite data for middle latitude regions of East Asia, *Progress in Natural Science*, *16*(10), 1084-1089.

Huang, J. P., et al. (2008), An Overview of the Semi-arid Climate and Environment Research Observatory

over the Loess Plateau, *Advances in Atmospheric Sciences*, *25*(6), 906-921, doi:10.1007/s00376-008-0906-7.

Illingworth, A. J., et al. (2007), Cloudnet - Continuous evaluation of cloud profiles in seven operational models using ground-based observations, *Bulletin of the American Meteorological Society*, *88*(6), 883-+, doi:10.1175/bams-88-6-883.

King, M. D., S. Platnick, W. P. Menzel, S. A. Ackerman, and P. A. Hubanks (2013), Spatial and Temporal Distribution of Clouds Observed by MODIS Onboard the Terra and Aqua Satellites, *Ieee Transactions on Geoscience and Remote Sensing*, *51*(7), 3826-3852, doi:10.1109/tgrs.2012.2227333.

Kollias, E. E. Clothiaux, M. A. Miller, B. A. Albrecht, G. L. Stephens, and T. P. Ackerman (2007a), Millimeter-wavelength radars - New frontier in atmospheric cloud and precipitation research, *Bulletin of the American Meteorological Society*, *88*(10), 1608-+, doi:10.1175/bams-88-10-1608.

Kollias, E. E. Clothiaux, M. A. Miller, E. P. Luke, K. L. Johnson, K. P. Moran, K. B. Widener, and B. A. Albrecht (2007b), The Atmospheric Radiation Measurement Program cloud profiling radars: Second-generation sampling strategies, processing, and cloud data products, *Journal of Atmospheric and Oceanic Technology*, *24*(7), 1199-1214, doi:10.1175/jtech2033.1.

Li, J., J. Huang, K. Stamnes, T. Wang, Q. Lv, and H. Jin (2015), A global survey of cloud overlap based on CALIPSO and CloudSat measurements, *Atmospheric Chemistry and Physics*, *15*(1), 519-536, doi:10.5194/acp-15-519-2015.

Mace, G. G., T. P. Ackerman, P. Minnis, and D. F. Young (1998), Cirrus layer microphysical properties derived from surface-based millimeter radar and infrared interferometer data, *Journal of Geophysical Research-Atmospheres*, *103*(D18), 23207-23216, doi:10.1029/98jd02117.

Mace, G. G., E. E. Clothiaux, and T. P. Ackerman (2001), The composite characteristics of cirrus clouds:

499 Bulk properties revealed by one year of continuous cloud radar data, *Journal of Climate*, *14*(10), 2185-
500 2203, doi:10.1175/1520-0442(2001)014<2185:tccocc>2.0.co;2.
501 Marchand, R., G. G. Mace, T. Ackerman, and G. Stephens (2008), Hydrometeor detection using Cloudsat
502 - An earth-orbiting 94-GHz cloud radar, *Journal of Atmospheric and Oceanic Technology*, *25*(4), 519-
503 533, doi:10.1175/2007jtecha1006.1.
504 Marr, D., and E. Hildreth (1980), THEORY OF EDGE-DETECTION, *Proceedings of the Royal Society*
505 *Series B-Biological Sciences*, *207*(1167), 187-217, doi:10.1098/rspb.1980.0020.
506 Perona, P., and J. Malik (1990), SCALE-SPACE AND EDGE-DETECTION USING ANISOTROPIC
507 DIFFUSION, *Ieee Transactions on Pattern Analysis and Machine Intelligence*, *12*(7), 629-639,
508 doi:10.1109/34.56205.
509 Protat, A., D. Bouniol, J. Delanoe, P. T. May, A. Plana-Fattori, A. Hasson, E. O'Connor, U. Goersdorf,
510 and A. J. Heymsfield (2009), Assessment of Cloudsat Reflectivity Measurements and Ice Cloud
511 Properties Using Ground-Based and Airborne Cloud Radar Observations, *Journal of Atmospheric and*
512 *Oceanic Technology*, *26*(9), 1717-1741, doi:10.1175/2009jtecha1246.1.
513 Protat, A., J. Delanoe, P. T. May, J. Haynes, C. Jakob, E. O'Connor, M. Pope, and M. C. Wheeler (2011),
514 The variability of tropical ice cloud properties as a function of the large-scale context from ground-based
515 radar-lidar observations over Darwin, Australia, *Atmospheric Chemistry and Physics*, *11*(16), 8363-8384,
516 doi:10.5194/acp-11-8363-2011.
517 Ramanathan, V., R. D. Cess, E. F. Harrison, P. Minnis, B. R. Barkstrom, E. Ahmad, and D. Hartmann
518 (1989), CLOUD-RADIATIVE FORCING AND CLIMATE - RESULTS FROM THE EARTH
519 RADIATION BUDGET EXPERIMENT, *Science*, *243*(4887), 57-63, doi:10.1126/science.243.4887.57.
520 Randall, D. A., R.A. Wood, S. Bony, R. Colman, T. Fichefet, J. Fyfe, V. Kattsov, A. Pitman, J. Shukla, J.

521 Srinivasan, R.J. Stouffer, A. Sumi and K.E. Taylor (2007), Cilmate Models and Their Evaluation. In:
522 Climate Change 2007: The Physical Science Basis, *Contribution of Working Group I to the Fourth*
523 *Assessment Report of the Intergovernmental Panel on Climate Change*, *[Solomon, S., D. Qin, M.*
524 *Manning, Z. Chen, M. Marquis, K.B. Averyt, M.Tignor and H.L. Miller (eds.)]*. *Cambridge University*
525 *Press, Cambridge, United Kingdom and New York, NY, USA.*
526 Sassen, K., and S. Benson (2001), A midlatitude cirrus cloud climatology from the facility for
527 atmospheric remote sensing. Part II: Microphysical properties derived from lidar depolarization, *Journal*
528 *of the Atmospheric Sciences*, *58*(15), 2103-2112, doi:10.1175/1520-
529 0469(2001)058<2103:amcccf>2.0.co;2.
530 Stephens, G. L. (2005), Cloud feedbacks in the climate system: A critical review, *Journal of Climate*,
531 *18*(2), 237-273, doi:10.1175/jcli-3243.1.
532 Stephens, G. L., et al. (2002), The cloudsat mission and the a-train - A new dimension of space-based
533 observations of clouds and precipitation, *Bulletin of the American Meteorological Society*, *83*(12), 1771-
534 1790, doi:10.1175/bams-83-12-1771.
535 Su, J., J. Huang, Q. Fu, P. Minnis, J. Ge, and J. Bi (2008), Estimation of Asian dust aerosol effect on
536 cloud radiation forcing using Fu-Liou radiative model and CERES measurements, *Atmospheric*
537 *Chemistry and Physics*, *8*(10), 2763-2771.
538 Thorsen, and Q. Fu (2015), Automated Retrieval of Cloud and Aerosol Properties from the ARM Raman
539 Lidar. Part II: Extinction, *Journal of Atmospheric and Oceanic Technology*, *32*(11), 1999-2023,
540 doi:10.1175/jtech-d-14-00178.1.
541 Thorsen, Q. Fu, and J. Comstock (2011), Comparison of the CALIPSO satellite and ground-based
542 observations of cirrus clouds at the ARM TWP sites, *Journal of Geophysical Research-Atmospheres*, *116*,

543 doi:10.1029/2011jd015970.

544 Thorsen; Fu, Q. N., Rob K.; Turner David D.; Comstock Jennifer M. (2015), Automated Retrieval of
545 Cloud and Aerosol Properties from the ARM Raman Lidar. Part I: Feature Detection, *JOURNAL OF*
546 *ATMOSPHERIC AND OCEANIC TECHNOLOGY*, *32*(11), 1977-1998, doi:10.1175/JTECH-D-14-
547 00150.1.

548 Tomasi, C., and R. Manduchi (1998), Bilateral Filtering for Gray and Color Images, *IEEE International*
549 *Conference on Computer Vision, Bombay, India*, doi:10.1109/ICCV.1998.710815.

550 Wang, Z., and K. Sassen (2001), Cloud type and macrophysical property retrieval using multiple remote
551 sensors, *Journal of Applied Meteorology*, *40*(10), 1665-1682, doi:10.1175/1520-
552 0450(2001)040<1665:ctampr>2.0.co;2.

553 Williams, K. D., and M. J. Webb (2009), A quantitative performance assessment of cloud regimes in
554 climate models, *Climate Dynamics*, *33*(1), 141-157, doi:10.1007/s00382-008-0443-1.

555 Yan, H. R., J. P. Huang, P. Minnis, Y. H. Yi, S. Sun-Mack, T. H. Wang, and T. Y. Nakajima (2015),
556 Comparison of CERES-MODIS cloud microphysical properties with surface observations over Loess
557 Plateau, *Journal of Quantitative Spectroscopy & Radiative Transfer*, *153*, 65-76,
558 doi:10.1016/j.jqsrt.2014.09.009.

559 Yuan, J., Q. Fu, and N. McFarlane (2006), Tests and improvements of GCM cloud parameterizations
560 using the CCCMA SCM with the SHEBA data set, *Atmospheric Research*, *82*(1-2), 222-238,
561 doi:10.1016/j.atmosres.2005.10.009.

562

Cloud Type	Performance (%)	Cloud Mask Confidence Level			
		≥10	≥20	≥30	≥40
Strong	False positive	0.048	0.044	0.009	0
	Failed negative	0.244	0.244	0.244	0.244
Moderate	False positive	0.103	0.103	0.063	0
	Failed negative	0.229	0.229	0.229	100
Weak	False positive	0.007	0.006	0.003	0
	Failed negative	9.774	96.788	100	100

563 Table 1. Summary of false positives and failed negatives for hypothetical strong,
564 moderate and weak cloud cases in Fig.4 a1, a2, and a3, respectively.

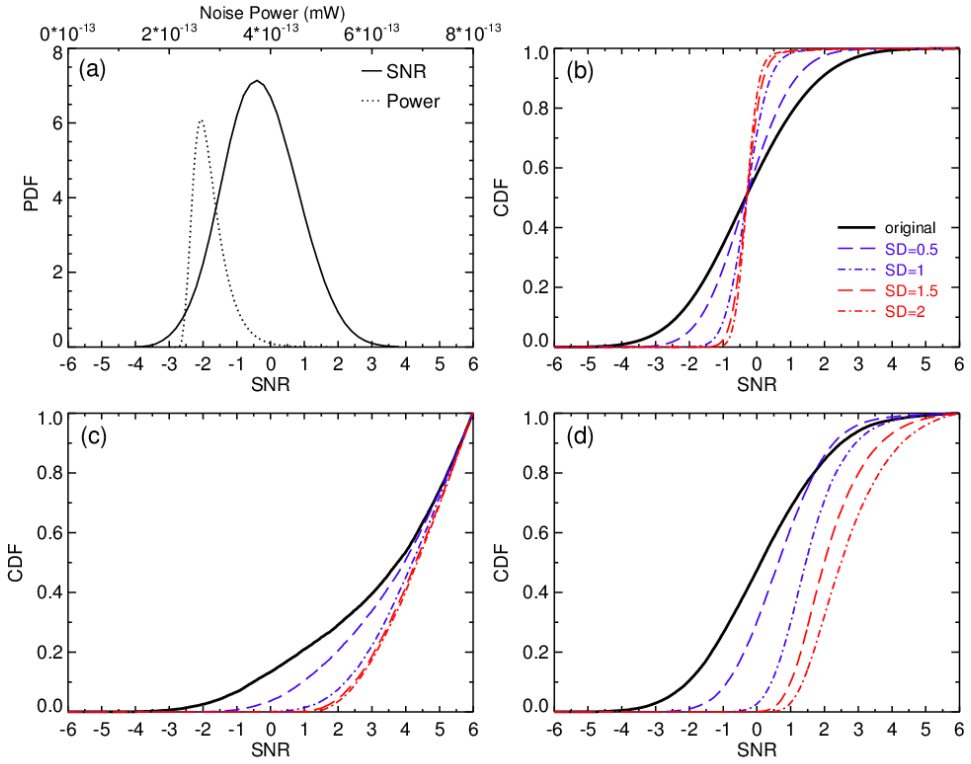

Figure 1. (a) Probability distribution function (PDF) of the noise power and SNR from the KAZR observations in a clear day of January 21, 2014. (b) Cumulative distribution function (CDF) of original and convolved SNR for the noise from the clear day. (c) and (d) CDF of original and convolved SNR from a cloudy case of January 4, 2014 for range gates inside and outside the cloud adjacent to the cloud boundary, respectively.

570

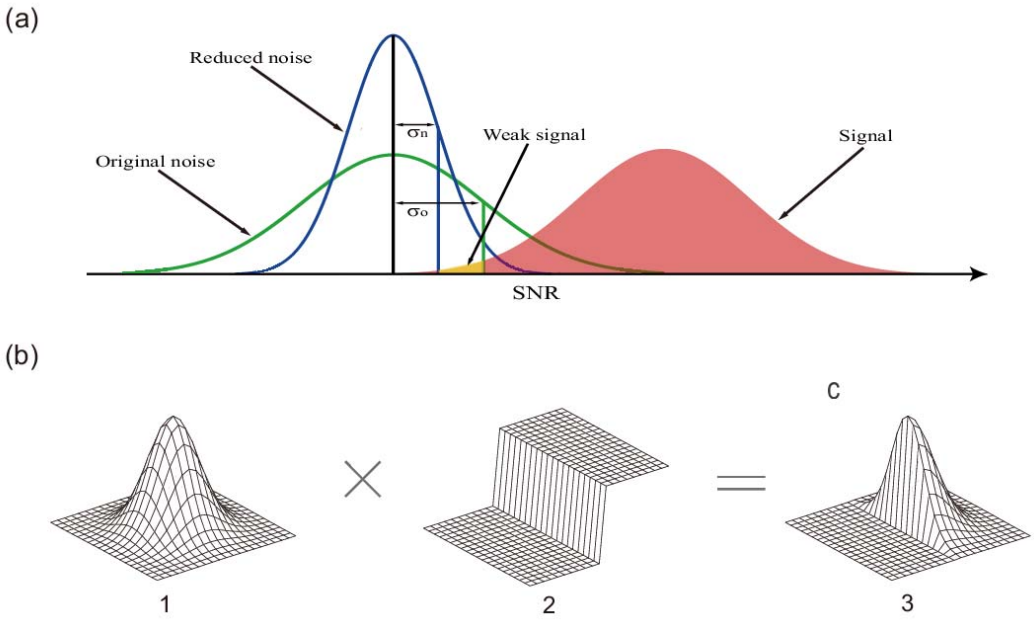

571 Figure 2. (a) comparison of original noise, reduced noise and hydrometeor signal
572 distributions. (b) Illustration of the bilateral filtering process. (b1) Gaussian kernel
573 distribution in space. (b2) δ function. (b3) Bilateral kernel by combining Gaussian
574 kernel with δ function.
575

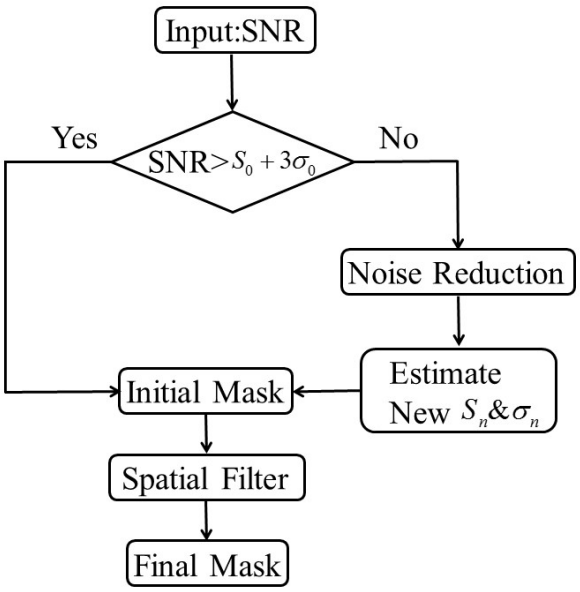

576 Figure 3. Schematic flow diagram for hydrometeor detection method.

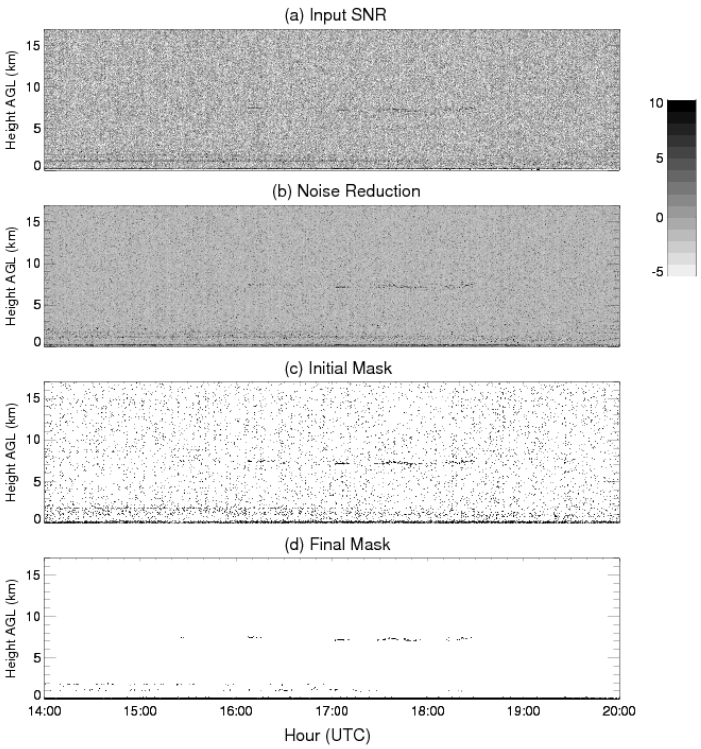

577

578 Figure 4. Illustration of the steps of the detection method using the real data of January

579 8th, 2014.

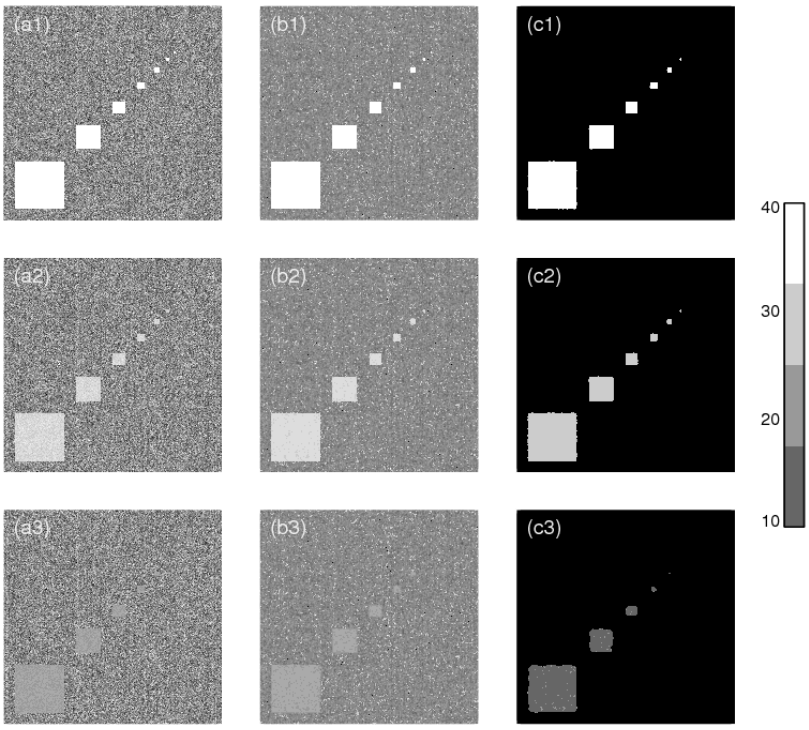

Figure 54. Panels a_1, a_2 and a_3 are three "square clouds" that have strong, moderate and weak SNR values with random Gaussian noise used to test the detection method. Panels b_1, b_2 and b_3 are SNR distributions after convolving the data with a bilateral kernel. Panels c_1, c_2 and c_3 are the final cloud mask filtered by the spatial filter.

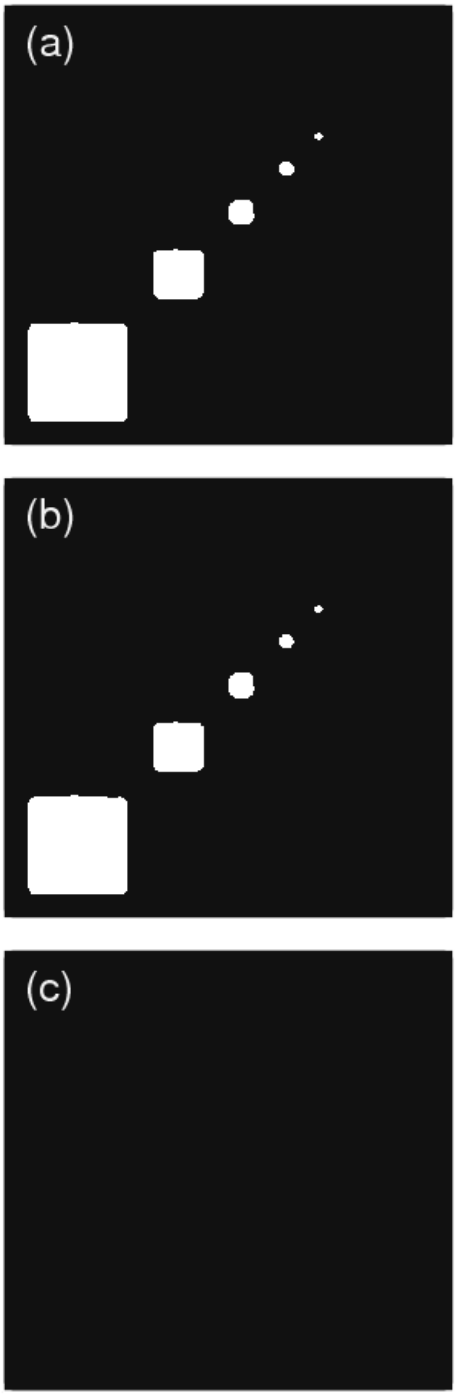

Figure 6~~5~~. Cloud mask without applying noise reduction and central pixel weighting. (a), (b), (c) are for the targets with strong, moderate and weak SNR, respectively, from Fig. 4 a1, a2, and a3.

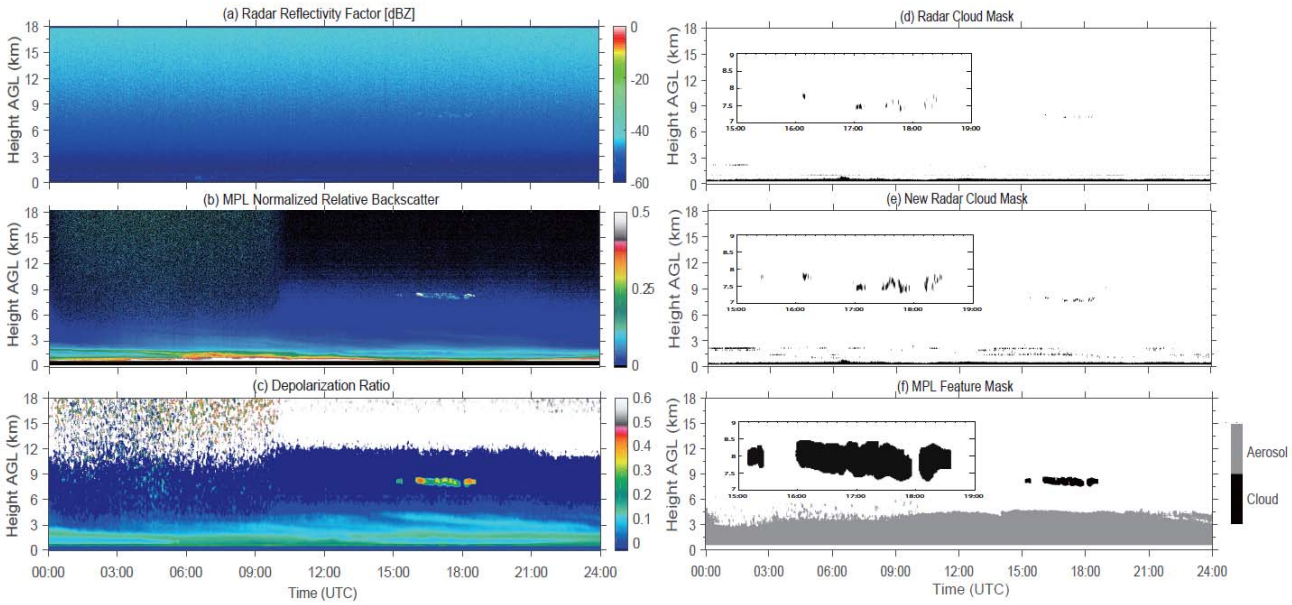

588 Figure 7~~6~~. One-day example of radar- and lidar-observed cirrus cloud at the SACOL
589 on January 8, 2014. (a) KAZR reflectivity. (b) MPL normalized backscatter intensity
590 ~~radar cloud mask derived by our new method.~~ (c)MPL Depolarization Ration ~~radar~~
591 ~~cloud mask derived by the ARM operational algorithm.~~ (d) radar cloud mask derived
592 by the ARM operational algorithm ~~MPL normalized backscatter intensity~~. (e) radar
593 cloud mask derived by our new method. (f) MPL feature mask. Three~~Two~~ windows in
594 (d~~b~~), (e~~e~~), (f) show the zoom-in views of cirrus masks.

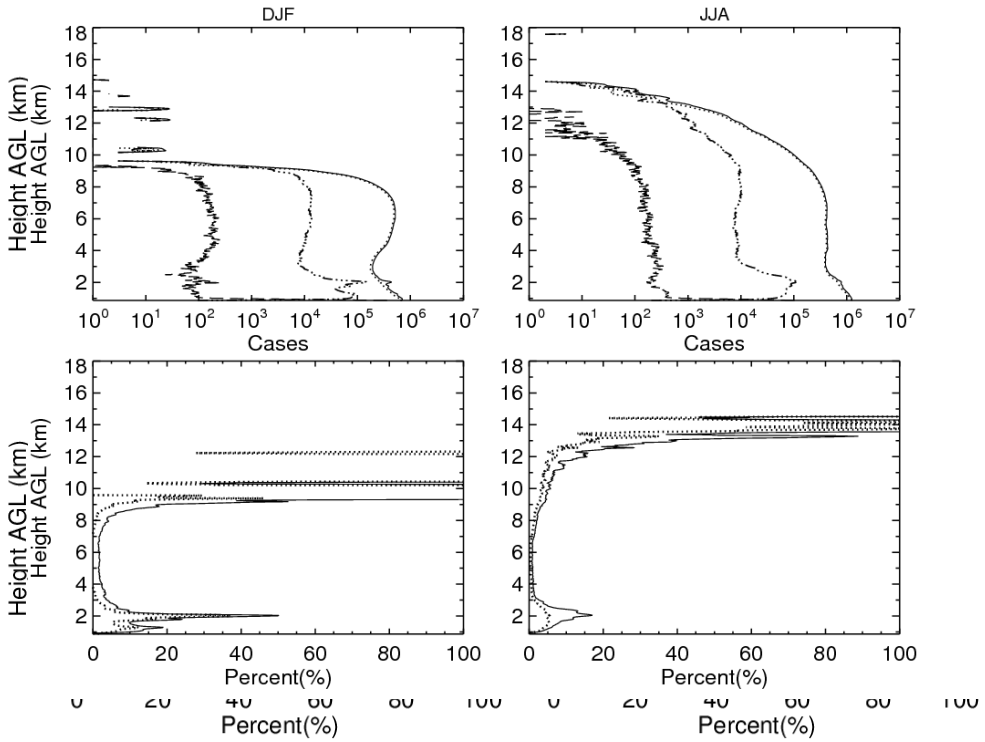

595 Figure 8~~7~~. The upper panel shows the number of occurrences of the detected
596 hydrometeor range bins from the two methods with the confusion matrix. The solid line
597 represents the results derived from our new method. The dot line represents the range
598 gate number that are detected as signals by both methods. The dashed line is the number
599 of range gates detected as noise by our method but signal by ARM. The dot-dash line
600 is the increased range gates from our method. The lower two panels demonstrate the
601 increased percentage of hydrometeor bins from our new method comparing to the ARM
602 operational method. The solid line is calculated by applying both noise reduction and
603 central-pixel weighting schemes, while the dashed line is calculated by only applying
604 the central-pixel weighting scheme in our detection method.
605

606 .

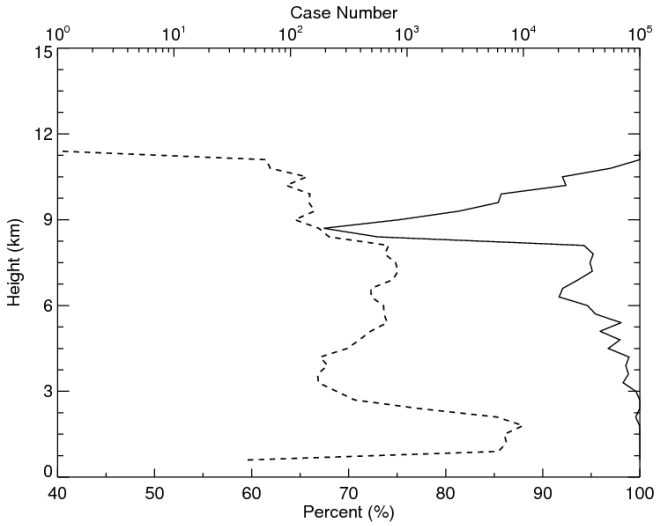

607 Figure 9. A comparison of the increased detections with the MPL observations. The
608 solid line is the percentage of increased detections seen by both KAZR with our method
609 and MPL as compared with the total increased detections. The dot line is the number of
610 increased detections.

611

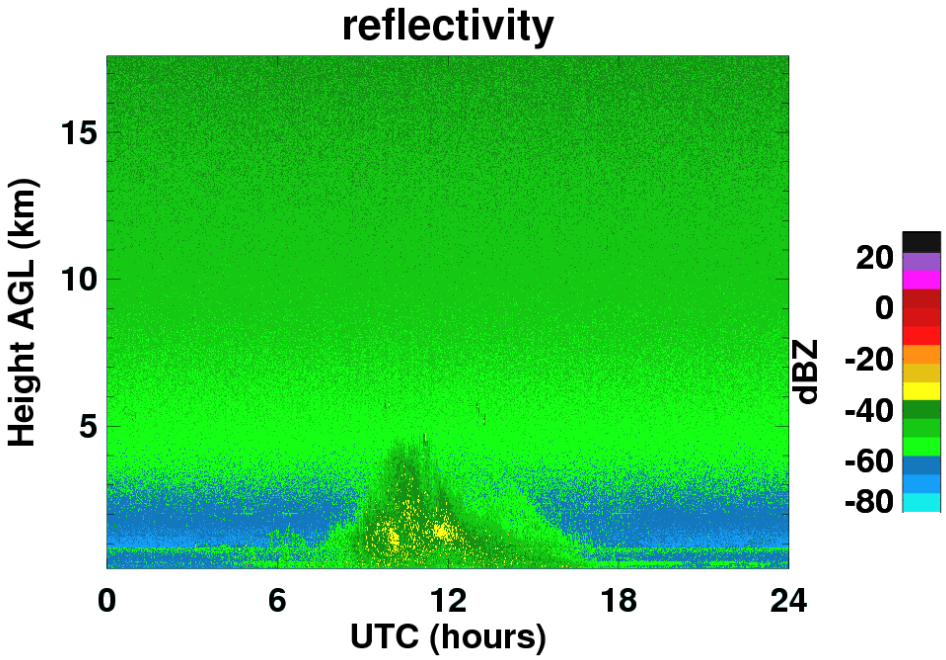

612 Auxiliary Figure 1. A dust event observed on January 29th, 2014. The morphology and

613 power level of the return signal is apparent not for a cloud from the surface to the height

614 of 5 km between 0800 to 1600 UTC.